



Contents lists available at ScienceDirect

European Journal of Medicinal Chemistry

journal homepage: <http://www.elsevier.com/locate/ejmech>

Research paper

Identification and characterization of benzo[d]oxazol-2(3H)-one derivatives as the first potent and selective small-molecule inhibitors of chromodomain protein CDYL

Lixin Yang^{a,1}, Yongqing Liu^{a,1}, Minghua Fan^a, Guiwang Zhu^a, Hongwei Jin^a, Jing Liang^b, Zhenming Liu^a, Zhuo Huang^{a,**}, Liangren Zhang^{a,*}^a State Key Laboratory of Natural and Biomimetic Drugs, School of Pharmaceutical Sciences, Peking University, Beijing, 100191, China^b Key Laboratory of Carcinogenesis and Translational Research (Ministry of Education), Department of Biochemistry and Molecular Biology, School of Basic Medical Sciences, Peking University, Beijing, 100191, China

ARTICLE INFO

Article history:

Received 3 July 2019

Received in revised form

24 August 2019

Accepted 28 August 2019

Available online 31 August 2019

Keywords:

CDYL

Benzo[d]oxazol-2(3H)-ones

Small-molecule inhibitors

Computer-aided drug design

SAR study

Dendritic morphogenesis

ABSTRACT

Chemical probes of epigenetic 'readers' of histone post-translational modifications (PTMs) have become powerful tools for mechanistic and functional studies of their target proteins in physiology and pathology. However, only limited 'reader' probes have been developed, which restricted our understanding towards these macromolecules and their roles in cells or animals. Here, we reported a structure-guided approach to develop and characterize benzo[d]oxazol-2(3H)-one analogs as the first potent and selective small-molecule inhibitors of chromodomain Y-like (CDYL), a histone methyllysine reader protein. The binding conformation between the chromodomain of CDYL and the modified peptidomimetics was studied via molecular docking and dynamic simulations, facilitating subsequent virtual screening of tens of hits from Specs chemical library validated by SPR technique (K_D values: from 271.1 μ M to 5.4 μ M). Further design and synthesis of 43 compounds helped to interpret the structure-activity relationship (SAR) that lead to the discovery of novel small-molecule inhibitors of CDYL. Compound **D03** (K_D : 0.5 μ M) was discovered and showed excellent selectivity among other chromodomain proteins, including CDYL2 (>140 folds), CDYL1 (no observed binding) and CBX7 (>32 folds). Moreover, we demonstrated that **D03** engaged with endogenous CDYL in a dose-dependent manner, and perturbed the recruitment of CDYL onto chromatin, resulting in transcriptional derepression of its target genes. Finally, the results showed that **D03** promoted the development and branching of neurodendrites by inhibiting CDYL in hippocampal and cortical cultured neurons. This study not only discovers the first selective small-molecule inhibitors of CDYL, but provides a new chemical tool to intervene the dynamic nature of bio-macromolecules involved in epigenetic mechanism.

© 2019 Elsevier Masson SAS. All rights reserved.

1. Introduction

Controlled regulation of gene expression is crucial for the development and function of multicellular organisms. Expression

of the genetic code is largely regulated by cell-type specific transcriptional factors, chemical modifications of DNA and histone proteins. The dynamic nature of epigenetics means that it may be possible to alter disease-associated epigenetic states through direct manipulation of the molecules involved in this process, which are metaphorically called 'writer', 'eraser', and 'reader' proteins [1,2]. With the development of the so-called epigenome, these proteins are increasingly in these years showing promising therapeutic relevance in multiple diseases like cancer, metabolic dysregulation and neuropsychiatric disorders, as well as in regenerative medicine [3–5]. Noticeably, many inhibitors of 'writer' proteins like histone methyltransferases (HMTs) have entered diverse clinical trials [6–12] and inhibitors of 'eraser' proteins have been approved and

* Corresponding author. State Key Laboratory of Natural and Biomimetic Drugs, Department of Medicinal Chemistry, School of Pharmaceutical Sciences, Peking University Beijing, 100191, China.

** Corresponding author. State Key Laboratory of Natural and Biomimetic Drugs, Department of Molecular and Cellular Pharmacology, School of Pharmaceutical Sciences, Peking University, Beijing, 100191, China.

E-mail addresses: huangz@hsc.pku.edu.cn (Z. Huang), liangren@bjmu.edu.cn (L. Zhang).

¹ L.Y. and Y.L. contributed equally to this work.

used clinically against multiple malignancies [13–15]. To date, however, very few ‘reader’ proteins have been successfully targeted by small-molecule ligands [16,17].

Chromodomain Y-like (CDYL) protein is a recently identified transcriptional corepressor that contains an N-terminal chromodomain and a C-terminal enoyl-coenzyme A hydratase/isomerase catalytic domain [18,19]. The CDY family in human genome encodes three proteins, CDY1, CDYL and CDYL2. CDYL and CDYL2 are widely expressed in mammals, while CDY1 shows testis-specific expression [20]. In addition, CDYL contains three splicing variants (a, b, c), among which CDYL1b is the major splicing variant. Only CDYL1b recognizes methyl-lysines through its chromodomain, which facilitates the specific association with histone methylated modifications such as H3K9me3 and H3K27me3, thereby inhibiting the expression of downstream related genes [21–23]. CDYL was originally identified as a key player in the regulation of mammalian spermatogenesis [24,25]. Recent years, it was put to the moonlight that CDYL can play essential roles in the central nervous system since a significant number of CDYL target genes were associated with the development and function of the nervous system, such as the brain-derived neurotrophic factor (BDNF) [26]. CDYL negatively regulates dendritic branching in hippocampal neurons, suggesting that CDYL acts as a regulator during early stages of neural development, such as neuronal migration [26,27]. Further studies by our collaborators showed that CDYL can suppress epileptogenesis in mice through binding to the regulatory element in the intron region of SCN8A and repression of axonal Nav1.6 sodium channel expression [28]. The newly released perspective disclosed that CDYL played a critical role in regulating stress-induced depression by repressing the expression of neuropeptide VGF [29]. All of the mentioned correlations between CDYL and neuronal activities are based on the molecular mechanism of its ‘reader’ function.

However, although CDYL has a defined chromodomain and important biological functions, no specific tools have been discovered to investigate its precise role and potential to be a pharmacological drug target. One approach to increase our knowledge of its regulatory mechanisms is through small-molecule perturbation [30]. Accordingly, chemical biology efforts focused on interpreting the function of lysine methylation with chemical tools have gained momentum, resulting in a number of freely available high-quality chemical probes, such as inhibitors for heterochromatin protein 1 (HP1) and chromobox homolog 7 (CBX7) [31–35]. However, little active ligands have been discovered targeting the CDY family proteins, especially for the CDYL subtype, which exhibited significant relevance to neuropsychiatric disorders as described above. Nevertheless, there are still some clues for potential druggability of CDYL coming from targeting efforts of other chromodomains, like CBX chromodomains. CBX7 is a member of PRC1 complex, which possesses a chromodomain facilitating the recognition to certain methylated modifications [36,37]. Recently, potent ligands for CBX7 inspired from its recognition mechanism with the H3K27me3 modification were developed using adaptively biased molecular dynamics simulations. The resulting peptidomimetic UNC3866 showed robust binding with CBX7 and moderate interactions with three members of the CDY family, CDYL1b, CDYL2 and CDY1 [38]. Although the affinity of optimized peptidomimetics against CDY family was promoted several folds in subsequent combinatorial chemistry optimization, their subtype selectivity was still barely satisfactory [39]. Besides, their use as chemical probes in exploring and characterizing CDYL biological functions remains unknown.

To fully elucidate the importance of CDYL in human diseases as well as its druggable potential, especially in neuronal events, subtype-selective chemical probes are very essential. Herein we report a structure-based design strategy to develop first potent and selective small-molecule inhibitors of CDYL. The design, synthesis,

and structure-activity relationship studies that lead to the discovery of novel inhibitors are described. We demonstrate that the lead compound **D03** engages with endogenous CDYL, and perturbs the recruitment of CDYL onto chromatin, subsequently resulting in transcriptional derepression of its target genes. Finally, **D03** promotes dendritic maturation in primary cultured neurons, consistent with the known ability of CDYL overexpression to restrict dendritic arborization. These small molecules bear the potential to be modified into chemical probes that explore the functions of CDYL and treat its related diseases.

2. Results and discussion

2.1. Isatin derivatives are identified as hit compounds targeting CDYL via docking-based virtual screening strategy

Given that the chromodomain of CDYL was a critical region to drive the transcription repression (Fig. S1) and biological activities of CDYL [25–29], we thus focused our study on its N-terminal chromodomain. In an attempt to precisely regulate the transcriptional repression activity of CDYL (CDYL1b isoform in our work), we need to screen and identify novel CDYL modulators. To date, the structure of CDYL protein has not been resolved, and there is only one NMR apo-structure (PDB ID: 2DNT) of its N-terminal chromodomain with 20 conformations different largely in the starting loop region. The conformation overlay indicated that the secondary structures were rather stable, which helped to form a hydrophobic cage composed of its residues Trp36, Tyr39 and Tyr14 of the starting loop (Fig. S2). The hydrophobic cage of CDYL chromodomain can specifically recognize H3K9/27me3 modifications by forming a tight cation- π stacking network with the trimethylated lysine mark [21]. This is a highly induced-fit process, and thus an energy-optimized binding model for CDYL is crucial to conduct docking-based screening. Recently, UNC3866 was identified as the peptidomimetic ligand of CBX7, and also exhibited micromolar binding affinity (K_D : 0.91 μ M) to CDYL chromodomain by isothermal titration calorimetry (ITC) [38]. We synthesized the peptidomimetic UNC3866 and found a K_D value of 5.6 μ M (Figs. S3A–B) with CDYL chromodomain via surface plasmon resonance (SPR). However, UNC3866 didn't affect the expression of CDYL target gene MYT1 in SH-SY5Y and HEK-293T cells, even in a concentration up to 200 μ M (Figs. S3C–D). Due to its strong affinity, we use UNC3866 as ligand to stabilize the conformation of CDYL chromodomain and discover novel small-molecule inhibitors through virtual screening.

The overall in silico modeling and virtual screening workflow was shown in Fig. 1A and the Specs chemical library containing over 200,000 molecules was employed in this study. Firstly, We docked peptidomimetic UNC3866 to the chromodomain functional site containing the conserved hydrophobic cage using the induced-fit docking module in Schrodinger 2018.1. The resulting binding model was afterwards used in a 20 ns molecular dynamic simulation to see the potential binding process between CDYL and UNC3866. As shown in Fig. 1B, the RMSD values of C α , Lig fit Prot, and Lig fit Lig gradually achieved stability after around 8 ns, which meant that the complex had reached an equilibrium state and the Gibbs energy of the system was low. So we selected the binding model in 10 ns to analyze detailed interactions and construct a relatively stable docking model (Fig. 1C).

Sixty-two compounds were picked out in the first-round screening (Fig. S4 and Table S1). Their binding affinity to CDYL and the transcriptional inhibition of its target genes were then tested. Most of the hits showed about 10–20 folds weaker affinity towards CDYL than UNC3866, ranging from 14.2 μ M to 271.1 μ M (Fig. 2A). Among them, those isatin derivatives like **AK-778**/

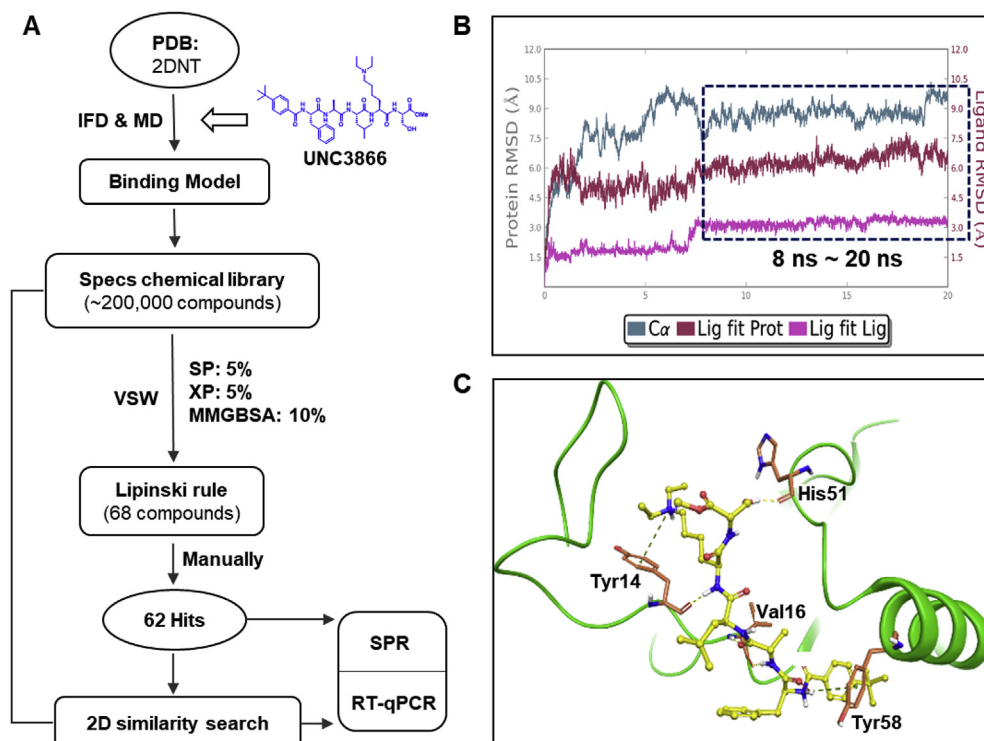


Fig. 1. A schematic diagram of in silico modeling and virtual screening. (A) Iterated virtual screening pipeline with detailed parameter setting. IFD, induced-fit docking; MD, molecular dynamics; VSW, virtual screening workflow; SP, standard precision; XP, extra precision. (B) Results of the 20 ns molecular dynamic simulations for CDYL-UNC3866 complex. (C) Energy-optimized binding model of CDYL-UNC3866 complex.

41051004 (Fig. 2B) exhibited more potent activity on gene expression (Fig. 2C), indicating greater potential as the hit compound to find better ligands with the similar scaffold.

For the second-round screening, we chose **AK-778/41051004** as a template to conduct rapidly shape-based 2D similarity search and get insight into the potential for isatin scaffold to be used as CDYL ligands. Over 200 compounds were thus screened out and around 1/4 of which were selected based on their similarity rankings. We also tested their binding affinity towards CDYL by SPR, as well as another three sequence highly conserved chromodomain proteins, CDYL2, CDYL1 and CBX7. The results showed that most of the active ligands possessed similar binding affinity to CDYL as the hits identified in the first round except **AK-778/41314725**, which exhibited comparative affinity (K_D : 4.9 μ M) with UNC3866. Moreover, it showed considerable subtype selectivity to CDYL against other chromodomain proteins (Table 1). Also, the RT-qPCR results demonstrated that it reversed the suppression of downstream gene expression in a dose-dependent manner (Fig. S5). Together, these results indicated that the isatin derivatives were competent to be potential inhibitors of the CDY family.

2.2. The hydroxyl group of the racemic AK-778/41314725 is not a necessary pharmacophore for CDYL binding and function

It is worthy of attention, however, all the purchased isatin derivatives were all racemic compounds, so we can't tell which enantiomer of the pair fitted better in the active site of CDYL chromodomain. Instead of obtaining the pure enantiomer via chemical resolution or chiral synthesis, we turned to remove the chiral center to simplify the core structure and see the real impact of the -OH upon binding to CDYL. As shown in Scheme 1, **AK-778/41314725** and its derivatives **A01**, **A02** and **A03** were synthesized, and their binding affinities to various chromodomains and their

cytotoxicity were evaluated.

The elimination of its hydroxyl group which yielded **A01** increased the molecular rigidity, and led to undesired toxicity. Also, its binding affinity was slightly weakened (K_D : 15.4 μ M). However, the reduction of **A01** to **A02** markedly increased the affinity (K_D : 1.2 μ M) towards CDYL while the toxicity still retained. Moreover, when the chiral carbon atom of **A02** was replaced with a nitrogen atom to yield **A03** which didn't possess a chiral center any more, the affinity decreased accordingly (K_D : 14.8 μ M), but its cytotoxicity decreased remarkably in HEK-293T and SH-SY5Y cells. Besides, **A03** retained its selectivity to CDYL among the four chromodomain proteins compared with **AK-778/41314725**. The results in Table 2 indicated that the hydroxyl group at the core structure was not a necessary moiety and can thus be removed to afford simplified lead compound in following structural modifications.

2.3. Compounds designed to form π - π stacking network interactions with the hydrophobic cage of CDYL chromodomain

With two-round virtual screening attempts, we discovered compound **A03** as a hit ligand of CDYL which showed considerable subtype selectivity. Then versatile structural modifications were made based on **A03** to get detailed understanding of the structure-activity relationship (see Schemes 2–5). As suggested in the induced-fit docking model of CDYL-**A03** complex (Fig. S6), the carbonyl group of **A03** formed tight hydrogen bonds with residues Leu 13 and Tyr14 of the starting loop region and stabilized its conformation. Although the methoxyphenyl group of **A03** communicated with the hydrophobic cage residues Tyr14, Trp36 and Tyr39 mainly through π - π stacking and hydrophobic interactions, it wasn't satisfactory since only Tyr14 formed desired π - π stacking with **A03**. Besides, the 2-benzoxazolinone fragment induced a new binding site in between of the flexible loop and the

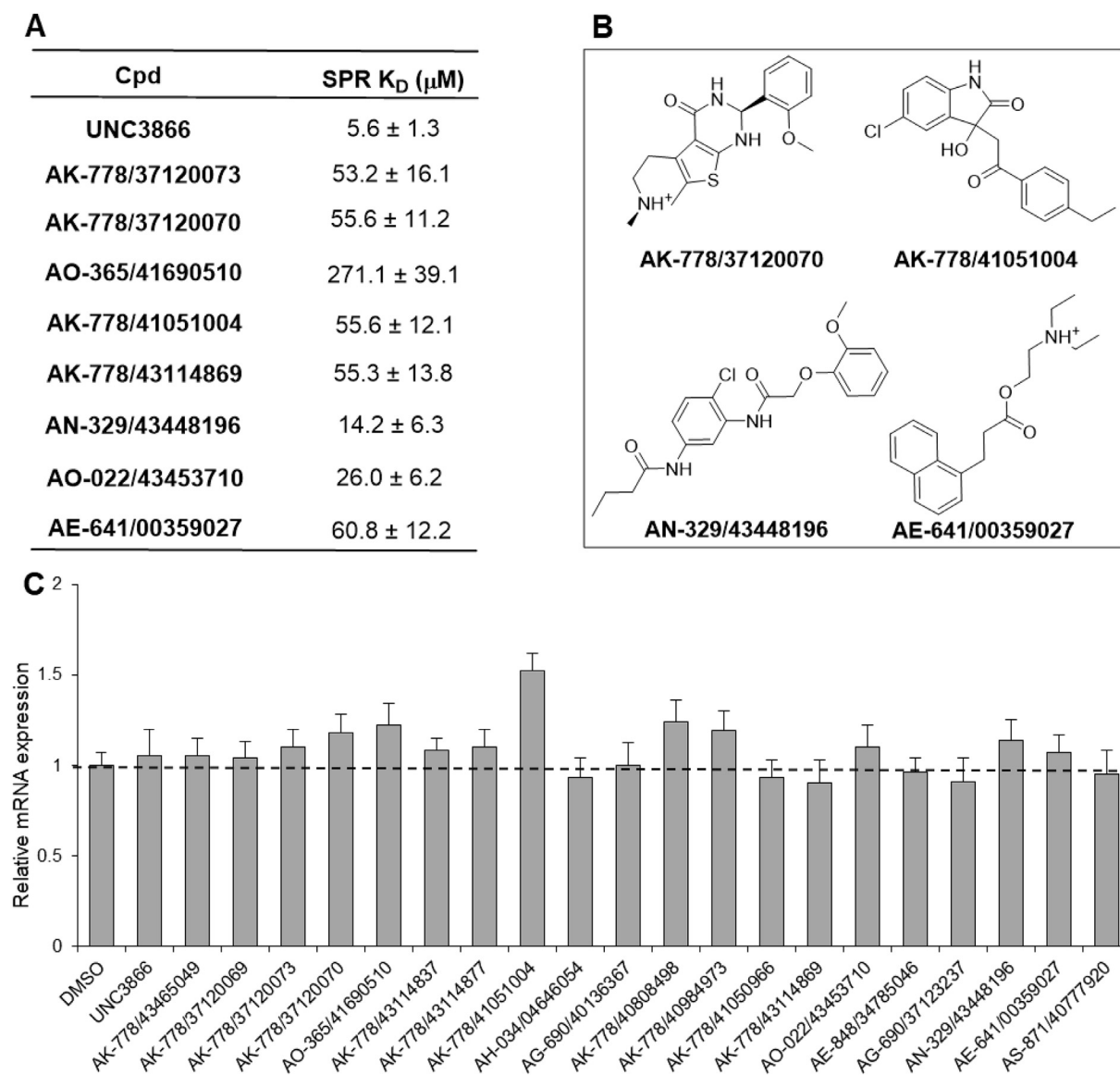


Fig. 2. Biological evaluation of hit compounds obtained in first round virtual screening. (A) Binding affinity with CDYL (K_D) determined by SPR. The K_D values were calculated as the mean \pm the standard deviation of at least two replicates each performed in duplicate. (B) The 2D structures of some representative hit compounds. (C) The mRNA expression of MYT1 in SH-SY5Y cells treated with 100 μ M compounds for 24 h. Each bar represents the mean \pm S.E.M. for triplicate experiments.

β -strand of CDYL, but it didn't form versatile types of interactions owing to its featureless aromatic structure.

Consequently, we further synthesized 29 derivatives based on the analysis of CDYL-A03 binding model. The synthesis of compounds **B01–B25** was shown in Scheme 2. The benzoxazolinone and benzothiazolinone intermediates were synthesized from commercially available substituted 2-aminophenol and 2-aminobenzenethiol. The α -Br ketone derivatives were obtained via addition of a α -position bromine catalyzed by CuBr. Then a nucleophilic substitution in the presence of K_2CO_3 at 60–70 $^\circ$ C between the two building blocks afforded compounds **B01–B25**. The same reaction was also used in the synthesis of compounds **B26–29** (Scheme 3).

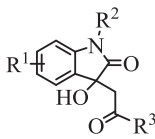
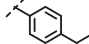
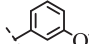
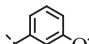
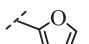
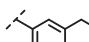
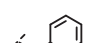
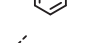
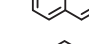
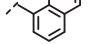
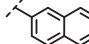
At first, the 2-benzoxazolinone scaffold of A03 was replaced by 2-benzothiazolinone, and whose 5-Cl was removed to get compound **B01**. Its binding affinity (K_D : 4.9 μ M) slightly increased by around 3 folds and maintained its selectivity to CDYL subtype. The influence of 5-position was also studied. Results in Table 3 showed

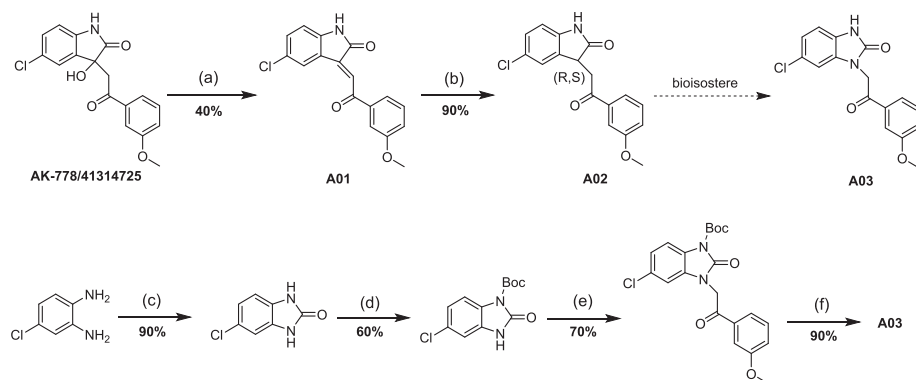
that bigger and/or more rigid group substitution of 5-position hindered their binding with CDYL and also affected the selectivity, like **B04**, whose affinity dramatically decreased when replaced by 5-CN. However, when the oxazolinone ring was augmented to a hexatomic ring, such as **B26** and **B27**, their binding affinity roughly retained and showed little difference to A03.

As implied in Table 3, when the 5-Cl was replaced by 5-F (**B02**) and 5-OCH₃ (**B03**), their binding affinity increased by 2 folds though occasionally changed their binding preference to other chromodomain proteins like CBX7 or CDYL2. So in subsequent modifications, we studied these substitutions one by one, and the methoxyphenyl group that interacted with the hydrophobic cage was also explored simultaneously. For the derivatives with a non-substituted benzoxazolinone group (**B05–B09**), results in Table 4 indicated that the binding affinity improved remarkably by around 2 folds when the benzene ring was replaced with larger aromatic rings, like the naphthalene of **B07** and **B08**, and indole of **B09**. Also, their subtype selectivity still retained accordingly. For

Table 1

The active compounds determined in shape screening and SPR.

Cpd				SPR K_D (μ M) ^a			
	R ¹	R ²	R ³	CDYL	CDYL2	CDY1	CBX7
AK-778/41051004	3-Cl	H		55.6 \pm 12.0	96.4 \pm 32.0	33.5 \pm 4.6	12.1 \pm 5.3
AK-778/43206467	H	n-Butyl		100 \pm 14.0	53.6 \pm 34.0	17.2 \pm 2.1	8.8 \pm 0.9
AK-778/41314725	3-Cl	H		4.9 \pm 0.3	n.d. ^b	n.d.	84.4 \pm 25.0
AK-778/43420918	H	i-Propyl		13.1 \pm 3.5	54.7 \pm 5.7	61.6 \pm 34.0	41.1 \pm 7.9
AK-778/43114937	H	n-Propyl		50.5 \pm 6.8	14.5 \pm 8.6	89.5 \pm 26.0	7.2 \pm 5.7
AK-778/43114894	H	n-Propyl		23.0 \pm 4.5	n.d.	21.1 \pm 3.3	20.4 \pm 3.2
AG-205/33681008	H	CH ₃		19.4 \pm 2.1	68.1 \pm 39.0	28.9 \pm 1.4	5.1 \pm 6.7
AK-778/43416943	H	CH ₃		128 \pm 50.0	>200 ^c	24.7 \pm 8.6	2.4 \pm 1.8
AK-778/41050965	H	Allyl		31.7 \pm 3.8	51.8 \pm 36.0	24.5 \pm 6.4	n.d.
AK-778/43465061	3-Cl	n-Propyl		15.4 \pm 0.9	n.d.	n.d.	16.0 \pm 7.1

^a The K_D values were calculated as the mean \pm the standard deviation of at least two replicates each performed in duplicate.^b Cannot be determined or not detected.^c The binding constants were weaker than 200 μ M.**Scheme 1.** Synthesis of compounds **A01–A03**, derivatives of **AK-778/41314725**. Reagents and conditions: (a). HAc, concentrated HCl, EtOH, 90 °C, then r.t., 0.5 h; (b). Pd/C, H₂, 3 bar, r.t., overnight; (c). CDI, DCM, r.t., 3 h; (d). Boc₂O, K₂CO₃, dry MeCN, r.t., 0.5 h, then reflux, 3 h; (e). 2-bromo-1-(3-methoxyphenyl)ethan-1-one, K₂CO₃, MeCN, 90 °C, 4.5 h; (f). HCl, THF, r.t., 2 h.

those with a 5-F substituted benzoxazolinone group (**B10–B13**), the results showed that their affinity towards CDYL was affected and dropped by around 4–5 folds when the benzene group was further decorated (**B10**, **B11**) or replaced with larger aromatic rings (**B12**, **B13**), indicating a preference binding for the original methoxyphenyl group. At the same time, their selectivity was also

disappeared. This problem maybe came from the molecular rigidity rooting from the short linker of the ligands and was expected to be studied. However, situations were totally different when the 5-position was replaced with the methoxy group such as compounds **B14–B17**. The results showed that these ligands normally retained their affinity to CDYL and even went beyond. For example,

Table 2
Chemical modifications based on the racemic compound **AK-778/41314725**.

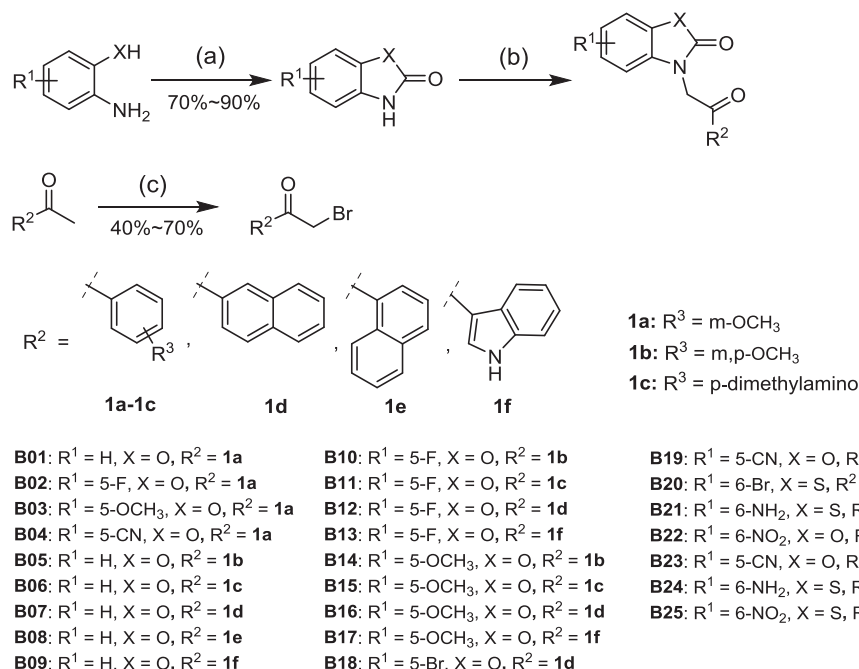
Cpd	SPR K_D (μ M) ^a				Cytotoxicity IC_{50} (μ M) ^b	
	CDYL	CDYL2	CDY1	CBX7	HEK-293T	SH-SY5Y
AK-778/41314725	4.9 \pm 0.3	n.d. ^c	n.d.	84.4 \pm 25.0	56.1 \pm 2.1	68.1 \pm 2.1
A01	15.4 \pm 3.7	4.3 \pm 2.7	10.3 \pm 4.6	n.d.	16.6 \pm 1.7	21.5 \pm 1.6
A02	1.2 \pm 0.8	19.7 \pm 3.2	>200 ^d	n.d.	36.9 \pm 1.4	43.4 \pm 2.1
A03	14.8 \pm 3.9	37.4 \pm 9.0	70.4 \pm 19.0	28.9 \pm 6.9	>200	>200

^a The K_D values were calculated as the mean \pm the standard deviation of at least two replicates each performed in duplicate.

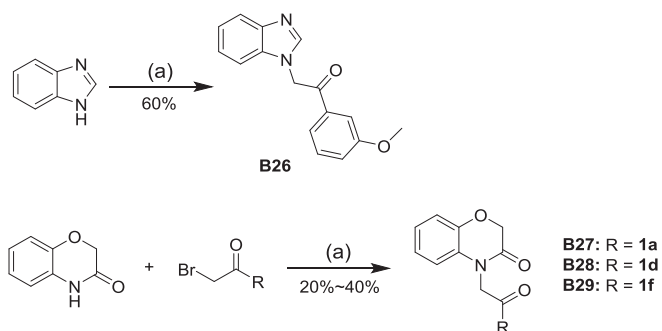
^b The IC_{50} values were reported as the mean \pm s.e.m of three biological replicates.

^c Cannot be determined or not detected.

^d The binding constants were weaker than 200 μ M.



Scheme 2. Synthesis of compounds **B01–B25**. Reagents and conditions: (a) CDI, DCM, r.t., 2 h; (b) 2-bromo-1-ones, K_2CO_3 , DMF, TBAI, 70 °C, 5 h; (c) CuBr, CH_3OH , reflux, 1 h.



Scheme 3. Synthesis of compounds **B26–B29**. Reagents and conditions: (a) 2-bromo-1-ones, K_2CO_3 , DMF, TBAI, 70 °C, 5 h.

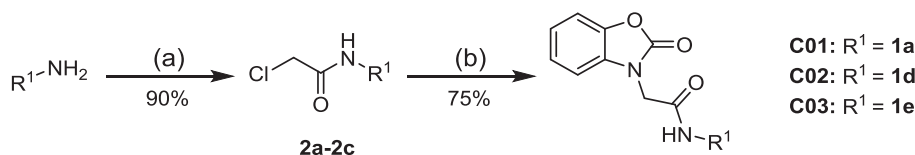
B14 (K_D : 5.5 μ M) and **B17** (K_D : 7.2 μ M) showed comparable binding affinity with **B03**, and the affinity of **B16** (K_D : 1.5 μ M) to CDYL even increased by 5 folds, although their subtype selectivity was slightly affected.

Taken together the results of Table 4, generally the hydrophobic cage of CDYL preferred larger aromatic groups which may contribute to the desired π - π stacking network. Subsequently, we

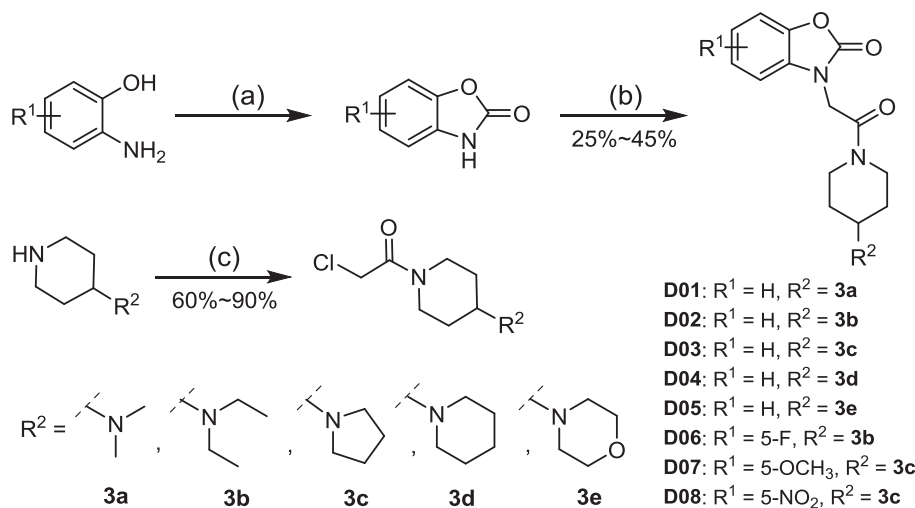
retained the naphthalene or indole group further and explored the substitutions of 5-/6-position again to enrich the SAR studies. For the ligands with a naphthalene group in Table 5, 5-Br substituted **B18** showed good binding affinity to all the chromodomains, especially for the CDYL2 subtype with a K_D value of 0.6 μ M. But for **B20** with a 6-Br group, its binding preference largely altered and showed better affinity to CDY1 subtype (K_D : 0.6 μ M), perhaps owing to the undesired steric hindrance. For **B19**, the poor binding affinity was consistent with the result got from **B04**, whose 5-CN showed negative effect for CDYL binding. For the benzothiazolinone derivatives with a 6-substituted $-NH_2/-NO_2$, their affinity to CDYL can be retained or just slightly decreased, like **B21** and **B22**, but their selectivity was totally in chaos. Besides, when the thiazolinone rings were augmented to oxazinone ones, their affinity and selectivity both abruptly decreased. The similar case was also found for the indole derivatives **B23–B25** (Table 6), among which only **B24** showed considerable binding affinity and preference for CDYL chromodomain.

2.4. Compounds designed to study the effect of molecular flexibility towards CDYL binding via modifying the chemical linker

As mentioned above, the linker in the core of the ligands may



Scheme 4. Synthesis of compounds **C01–C03**. Reagents and conditions: (a), chloroacetyl chloride, Et₃N, THF, ice-r.t., 8 h; (b), 2-chloro-N-R¹-acetamide, K₂CO₃, DMF, 70 °C, 5 h.



Scheme 5. Synthesis of compounds **D01–D08**. Reagents and conditions: (a) CDI, DCM, r.t., 2 h; (b) K₂CO₃, DMF, 70 °C, 5 h; (c) chloroacetyl chloride, Et₃N, THF, ice-r.t., 8 h.

Table 3

Binding affinity studies for compounds **B01–B04**, and **B26**, **B27**.

Cpd	R	SPR K _D (μM) ^a			
		CDYL	CDYL2	CDY1	CBX7
B01	H	4.9 ± 0.9	30.5 ± 4.8	5.8 ± 3.2	n.d.
B02	F	6.2 ± 1.5	28.7 ± 21.0	n.d.	3.4 ± 2.0
B03	OCH ₃	7.7 ± 3.3	3.4 ± 1.5	15.6 ± 6.4	17.2 ± 2.4
B04	CN	n.d. ^b	9.5 ± 2.1	42.1 ± 11.0	19.6 ± 12.0
B26	...	10.1 ± 2.7	56.2 ± 39.0	4.0 ± 2.0	n.d.
B27	...	13.0 ± 9.3	35.8 ± 11.0	11.3 ± 3.9	53.0 ± 7.6

^a The K_D values were calculated as the mean ± the standard deviation of at least two replicates each performed in duplicate.

^b Cannot be determined or not detected.

^c Structures were shown in [Scheme 3](#).

contribute greatly to the molecular rigidity, so we also attempted to interpret its role upon binding to the CDYL protein. A nitrogen atom was thus tentatively introduced in the original acetyl linker by forming an amide bond, which not only extended the length of the linker, but also added to its flexibility. For the synthesis of compounds **C01–C03**, aromatic amine groups were acetylated by chloroacetyl chloride at room temperature to yield 2-Cl substituted intermediates. Then they reacted with 2-benzoxazolinone to afford **C01–C03** by nucleophilic substitution ([Scheme 4](#)).

However, compared to **B01**, **B07** and **B08**, no indications of affinity increase to CDYL were observed for **C01–C03** ([Table 7](#)).

Instead, some of these ligands (**C01** and **C03**) showed exceptionally good binding affinity and preference to the CDY1 subtype. This can be further studied in the future.

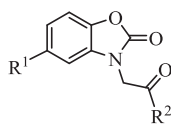
2.5. Compounds designed to form cation- π stacking network interactions with the hydrophobic cage of CDYL chromodomain

We concluded from the 32 derivatives discussed above that it was not necessary to retain the trimethylated marks of histone or diethylamine groups of UNC3866 to achieve specific binding with the hydrophobic cage of CDYL chromodomain. Many promising ligands like **B07**, **B08**, **B16** and **B21** also showed excellent affinity to CDY proteins as well as their binding selectivity. To fully understand the SAR of synthesized compounds, the cation- π network imitating the interaction between the methylated lysine marks and the hydrophobic cage was explored simultaneously.

We designed another 8 compounds with a fatty tertiary amine group, **D01–D08**. Compounds **D01–D08** were synthesized as shown in [Scheme 5](#). The secondary amine groups of piperidine derivatives were acetylated in ice shower by the dropwise added chloroacetyl chloride. Then the α -Cl of the intermediates were substituted by the 2-benzoxazolinone derivatives to yield the target compounds. Noticeably, the method for separation and purification in this scheme were much different from the compounds described above (see the Experimental Section).

The alkylated forms of the amine were chosen mainly in view of the cage volume and predicted cation- π stacking interactions ([Table 8](#)). For compounds **D01–D04**, most of them can bind well to CDYL, even slightly decreased affinity for **D01** (K_D: 9.5 μM) and **D04** (K_D: 11.8 μM) compared with **B01** (K_D: 4.9 μM). The results indicated that a tailored size of these tertiary amine fragments was necessary for potent CDYL targeting, such as **D03** (K_D: 0.5 μM). As a contrast, **D05** didn't exhibit good binding affinity to the CDYL

Table 4
Binding affinity studies for compounds **B05**–**B17**.



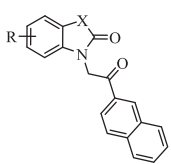
Cpd	R ¹	R ²	SPR K _D (μM) ^a			
			CDYL	CDYL2	CDY1	CBX7
B05	H		14.6 ± 8.9	5.3 ± 3.2	23.8 ± 11.0	48.5 ± 9.1
B06	H		11.9 ± 5.9	n.d. ^b	n.d.	36.5 ± 8.4
B07	H		2.6 ± 1.0	37.9 ± 1.2	41.7 ± 12.1	14.2 ± 4.0
B08	H		3.0 ± 0.3	24.1 ± 7.0	6.5 ± 2.1	29.9 ± 6.4
B09	H		1.9 ± 0.1	2.7 ± 0.4	21.0 ± 9.3	9.3 ± 3.6
B10	F		20.5 ± 8.3	73.7 ± 35.6	4.4 ± 1.0	28.8 ± 11.0
B11	F		90.1 ± 32.0	30.2 ± 7.4	34.6 ± 12.0	78.1 ± 9.2
B12	F		20.1 ± 1.9	n.d.	210 ± 41.0	40.2 ± 18.0
B13	F		5.1 ± 1.1	14.1 ± 3.2	23.7 ± 14.0	9.8 ± 6.6
B14	OCH ₃		5.5 ± 2.6	5.0 ± 0.6	11.3 ± 0.7	3.9 ± 2.9
B15	OCH ₃		15.5 ± 1.6	6.2 ± 3.4	2.7 ± 0.1	6.1 ± 1.7
B16	OCH ₃		1.5 ± 0.5	6.3 ± 1.6	1.5 ± 0.9	59.5 ± 11.0
B17	OCH ₃		7.2 ± 3.7	22.0 ± 7.6	36.4 ± 16.0	20.3 ± 5.7

^a The K_D values were calculated as the mean ± the standard deviation of at least two replicates each performed in duplicate.

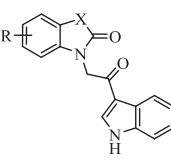
^b Cannot be determined or not detected.

family. Based on **D03**, the most potent and selective ligand, we designed the 5-position substituted derivatives like **D07** and **D08**. Their affinity and selectivity towards CDYL were significantly impaired. For compound **D06**, it surprisingly exhibited better

binding affinity to all the chromodomain proteins compared with **D02**, which showed good subtype selectivity to CDYL and CDYL2.

Table 5Binding affinity studies for compounds **B18–B22**, and **B28, B29**.


Cpd	R	X	SPR K_D (μM) ^a			
			CDYL	CDYL2	CDY1	CBX7
B18	5-Br	O	5.8 ± 0.8	0.6 ± 0.1	14.8 ± 7.9	9.5 ± 1.1
B19	5-CN	O	101 ± 12.2	n.d. ^b	71.5 ± 6.8	n.d.
B20	6-Br	O	29.0 ± 11.0	n.d.	1.7 ± 1.0	29.7 ± 17.0
B21	6-NH ₂	S	4.9 ± 1.9	13.7 ± 7.5	n.d.	>200 ^c
B22	6-NO ₂	S	26.8 ± 5.3	57.8 ± 27.0	123 ± 27.0	n.d.
B28	52.5 ± 12.0	11.9 ± 1.1	39.6 ± 4.7	26.5 ± 17.0
B29	59.8 ± 25.0	5.9 ± 1.3	109 ± 63.0	37.1 ± 17.0

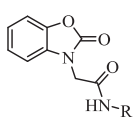
^a The K_D values were calculated as the mean ± the standard deviation of at least two replicates each performed in duplicate.^b Cannot be determined or not detected.^c The binding constants were weaker than 200 μM .^d The structures were shown in Scheme 3.**Table 6**Binding affinity studies for compounds **B23–B25**.


Cpd	R	X	SPR K_D (μM) ^a			
			CDYL	CDYL2	CDY1	CBX7
B23	5-CN	O	96.7 ± 38.0	2.8 ± 0.4	4.6 ± 1.6	46.9 ± 11.0
B24	6-NH ₂	S	3.5 ± 0.3	84.5 ± 19.0	51.1 ± 13.0	6.5 ± 2.1
B25	6-NO ₂	S	71.7 ± 12.0	3.8 ± 1.6	14.4 ± 3.3	8.8 ± 6.7

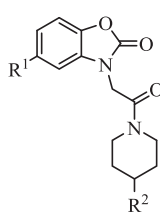
^a The K_D values were calculated as the mean ± the standard deviation of at least two replicates each performed in duplicate.

2.6. The SAR summary for structural optimizations

In above structural optimizations, we divided the main structure briefly into three parts, namely the induced pocket binding part, the linker part, and the hydrophobic cage binding part. To fit the hydrophobic cage, two kinds of compounds which were expected to form π - π or cation- π stacking interactions (Fig. 3A) were designed respectively. Fig. 3B illustrated the structure-activity relationship in terms of the molecular binding by SPR assay for the 40 synthesized compounds. In brief, for the induced binding part, chemical modifications in 5-/6-position of the compounds were mainly studied. The results implied that smaller substitutions at 5-position like 5-H/F contributed to the improved binding affinity while the less explored 6-position didn't show significant impact on the binding. For the fragment which can bind to the hydrophobic cage of CDYL, the binding nature depended on the types of the interactions. In general, bigger aromatic fragments such as naphthalene and indole rings predominantly increased the binding ability of the ligands by forming a π - π stacking network. Moreover, when the interactions switched from the π - π stacking network to a well-established cation- π stacking network, their binding affinity can further increase by around 5 folds. Other optimizations for the linker part were little but still attractive since compounds with

Table 7Binding affinity studies for compounds **C01–C03**.


Cpd	R	SPR K_D (μM) ^a			
		CDYL	CDYL2	CDY1	CBX7
C01		7.3 ± 1.0	7.2 ± 3.3	1.0 ± 0.5	14.8 ± 12.0
C02		18.9 ± 1.9	21.5 ± 4.6	20.4 ± 2.7	19.6 ± 7.9
C03		29.0 ± 4.3	5.8 ± 4.2	0.8 ± 0.2	>200 ^b

^a The K_D values were calculated as the mean ± the standard deviation of at least two replicates each performed in duplicate.^b The binding constants were weaker than 200 μM .**Table 8**Binding affinity studies for compounds **D01–D08**.


Cpd	R ¹	R ²	SPR K_D (μM) ^a			
			CDYL	CDYL2	CDY1	CBX7
D01	H		9.5 ± 4.0	>200 ^b	33.6 ± 13.0	n.d. ^c
D02	H		5.8 ± 2.0	4.7 ± 1.3	n.d.	46.6 ± 2.2
D03	H		0.5 ± 0.2	72.3 ± 11.2	n.d.	16.2 ± 3.8
D04	H		11.8 ± 1.3	84.5 ± 3.4	51.1 ± 12.0	13.5 ± 0.9
D05	H		25.9 ± 2.5	57.9 ± 8.6	21.0 ± 4.6	5.6 ± 0.8
D06	F		2.8 ± 1.2	3.4 ± 0.4	4.5 ± 1.8	2.8 ± 1.6
D07	OCH ₃		12.5 ± 8.9	2.1 ± 0.1	n.d.	8.2 ± 0.9
D08	NO ₂		16.8 ± 9.8	5.2 ± 0.6	55.8 ± 15.0	n.d.

^a The K_D values were calculated as the mean ± the standard deviation of at least two replicates each performed in duplicate.^b The binding constants were weaker than 200 μM .^c Cannot be determined or not detected.

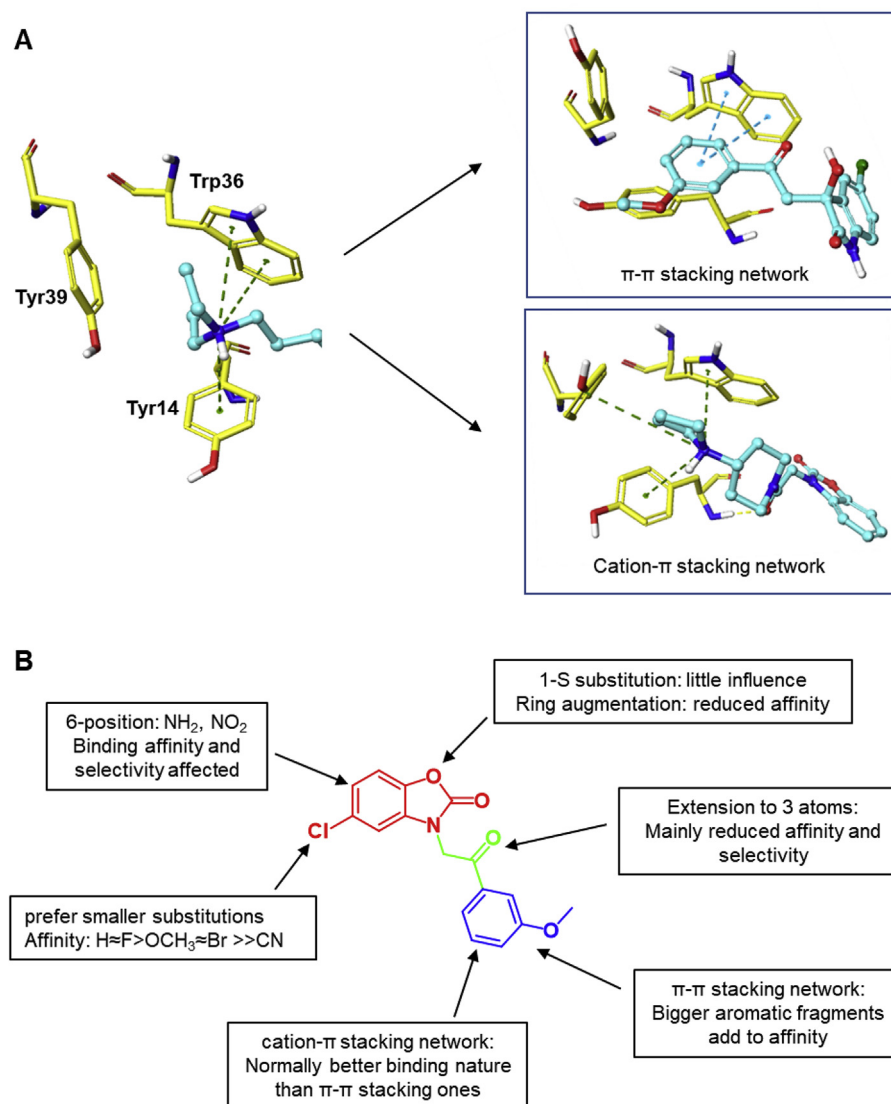


Fig. 3. Design rationales and the brief SAR gained from versatile structural modifications. (A) The π - π stacking network and cation- π stacking network designed to fit the hydrophobic cage of CDYL chromodomain. (B) The brief SAR gained from versatile structural modifications.

better binding affinity and preference to CDYL may be achieved by delicate design on this fragment, which should play a key role for the molecular flexibility of target ligands.

2.7. Compounds **B07** and **D03** lead to transcriptional derepression of CDYL target genes in SH-SY5Y and HEK-293T cells

Compounds **B07** and **D03**, the best ligands ever determined in comprehensive consideration of their excellent binding affinity and preference to CDYL, were thus expected to be studied in a series of biological assays related to CDYL function. As CDYL was demonstrated to mainly function as a transcriptional repressor [19,28], we firstly focused the effect of **B07** and **D03** on transcriptional activity of CDYL. Previous research showed that deletion of CDYL chromodomain resulted in an increase of MYT1/BDNF/VGF transcription levels [22,26,29]. By using real-time quantitative PCR, we indeed observed that the mRNA levels of MYT1/BDNF/VGF gradually increased in human SH-SY5Y cells upon dose-dependent treatment of **B07** (Fig. 4A) or **D03** (Fig. 4B) for 24 h. In addition, compared with the DMSO control, the transcript levels of MYT1/BDNF/VGF

stepwisely increased in HEK-293T cells after 24 h treatment of **B07** (Fig. 4D) or **D03** (Fig. 4E). However, treatment of compound **D07** performing weak binding affinity to CDYL did not affect the transcriptional levels of MYT1/BDNF/VGF in SH-SY5Y (Fig. 4C) or HEK-293T cells (Fig. 4F). Together, these data suggest that **B07** and **D03** can lead to transcriptional derepression of CDYL target genes in SH-SY5Y and HEK-293T cells.

2.8. Compound **D03** disrupts the recruitment of CDYL onto chromatin

Small-molecule inhibitors can perturb protein function and increase the protein stability via forming a ligand-protein complex. Thus, we attempted to investigate whether compound **D03** could bind to CDYL protein and increase its stability in cells. Through cellular thermal shift assay (CETSA), we found that **D03** treatment efficiently protected CDYL protein from temperature-dependent degradation in SH-SY5Y cells (Fig. 5A). Additionally, our data also demonstrated a dose-dependent reduced CDYL degradation with the incubation of **D03** (Fig. 5B), supporting that there is a direct

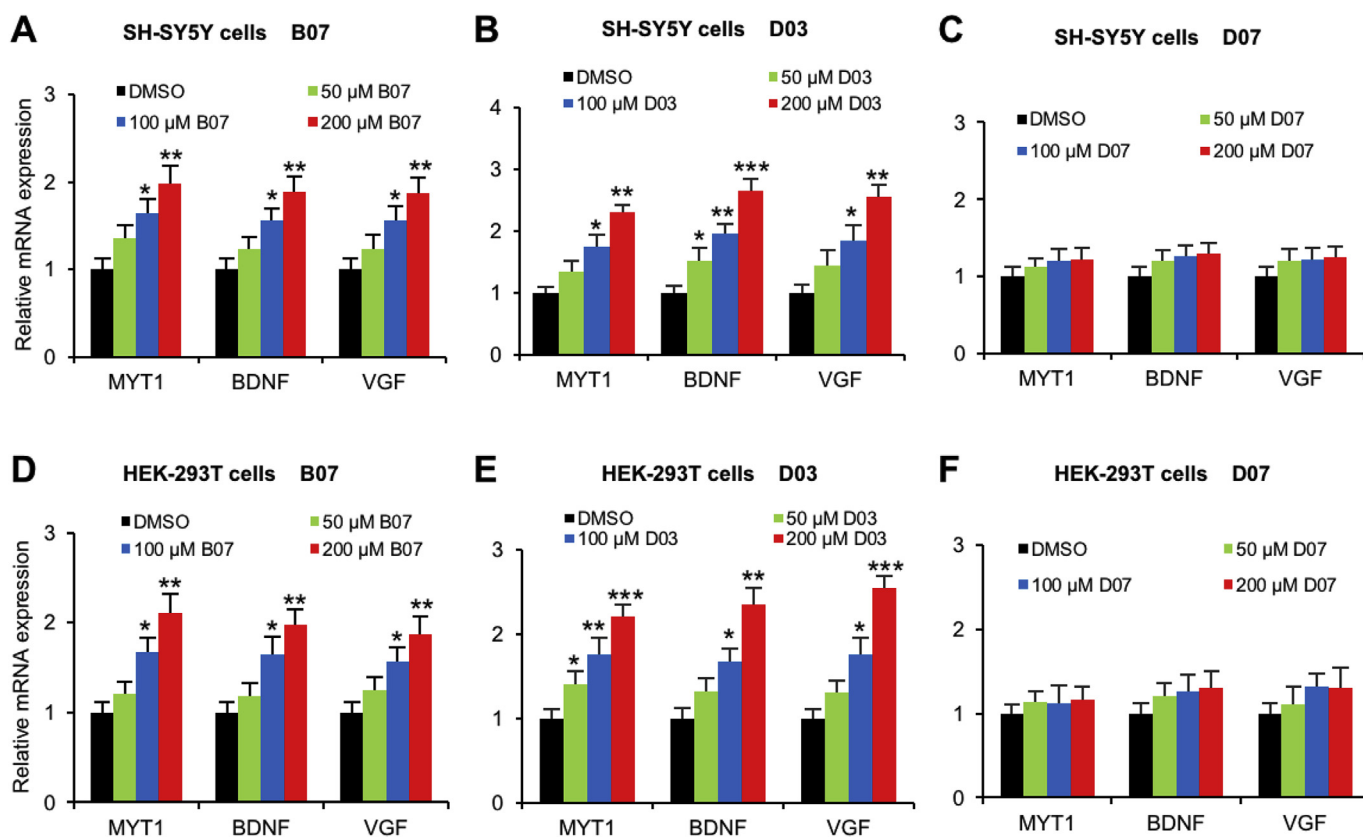


Fig. 4. Compounds **B07** and **D03** lead to transcriptional derepression of CDYL target genes. RT-qPCR analysis shows mRNA levels of CDYL target genes in SH-SY5Y cells (A–C) and HEK-293T cells (D–F) treated with **B07**, **D03** and **D07** respectively for 24 h. Each bar represents the mean \pm S.E.M. for triplicate experiments. *P*-values were determined by Student's *t*-test. **P* < 0.05, ***P* < 0.01, ****P* < 0.001.

interaction between **D03** and CDYL. Given that CDYL regulates its target genes transcription through its chromodomain-dependent association with chromatin. We next examined whether **D03** could perturb the CDYL-chromatin interaction and thereby modulate gene transcription. Using chromatin immunoprecipitation and quantitative PCR (ChIP-qPCR), we detected the decreases in the abundance of CDYL at its several target genes, such as MYT1, BDNF and VGF, in SH-SY5Y cells treated with 150 μ M **D03** (Fig. 5C), suggesting that engagement of the inhibitor could indeed prevent the enrichment of CDYL on its targeted genes. Furthermore, significantly decreased enrichment of H3K27me3 on MYT1/BDNF/VGF promoter were found in SH-SY5Y cells treated with 150 μ M **D03**, whereas the enrichment of CDYL and H3K27me3 on HOXA3 promoter, a non-CDYL target [23], were not altered in the above condition (Fig. 5C). The observed decrease of H3K27me3 matched the previous studies showing localized decreased H3K27me3 when CDYL was silenced. Collectively, the above data demonstrate that **D03** can disrupt the recruitment of CDYL onto chromatin, subsequently resulting in transcriptional derepression of its target genes.

2.9. Compound D03 promotes dendritic maturation in primary cultured neurons

Previous study reported that CDYL restricted dendrite arborization by repressing BDNF expression [26]. The neuropeptide VGF was induced by BDNF and promoted hippocampal dendritic maturation [40,41], as well as synaptic activity [41]. And MYT1 overexpression in the dentate gyrus induced an increase of BDNF expression, showing there was a positive correlation between MYT1 and BDNF [42]. Based on the clear mechanism of CDYL in the

regulation of dendritic morphogenesis, we next examined whether compound **D03** regulates dendritic branching. After treatment with **D03** for 24 h, the mRNA levels of MYT1/BDNF/VGF was significantly increased in cultured mouse hippocampal neurons (Fig. 6A) and cortical neurons (Fig. 6B), compared with the DMSO control. In addition, we observed a significant increase of dendritic branching compared with the control group (Fig. 6C–F). Clearly, these results suggest that compound **D03** promotes dendritic maturation in cultured neurons by blocking CDYL binding to its target genes.

2.10. Analysis of binding models for CDYL-B07/D03 complex

Compared with **D03**, compound **B07** possesses comparable and similar binding nature with CDYL family, indicating that the tertiary or quaternary amine groups designed for cation- π stacking interactions are not an exclusive feature for inhibition of Kme3 readers. When looking into the binding details of CDYL with **B07** and **D03** via induced-fit docking studies, we saw the detailed mechanism of action. As shown in Fig. 7A–C, the naphthalene group of compound **B07** bound to the hydrophobic cage in networked π - π stacking interactions with Trp36; a salt bridge between Glu11 and Asn 54 was then induced by the benzoxazolone part of the compound and buried it deep into the pocket. As a contrast, the ionized tertiary amine group of **D03** was tightly bound to the same hydrophobic cage via a cation- π network with residues Tyr14, Trp36 and Tyr39. A similar salt bridge was also induced by the benzoxazolone fragment, but it was between residues Glu11 and Hip 51 instead (Fig. 7D–F). However, to further enrich SAR studies of CDYL inhibition, more structural modifications should be scheduled. For example, bigger chemical space need to be enlarged

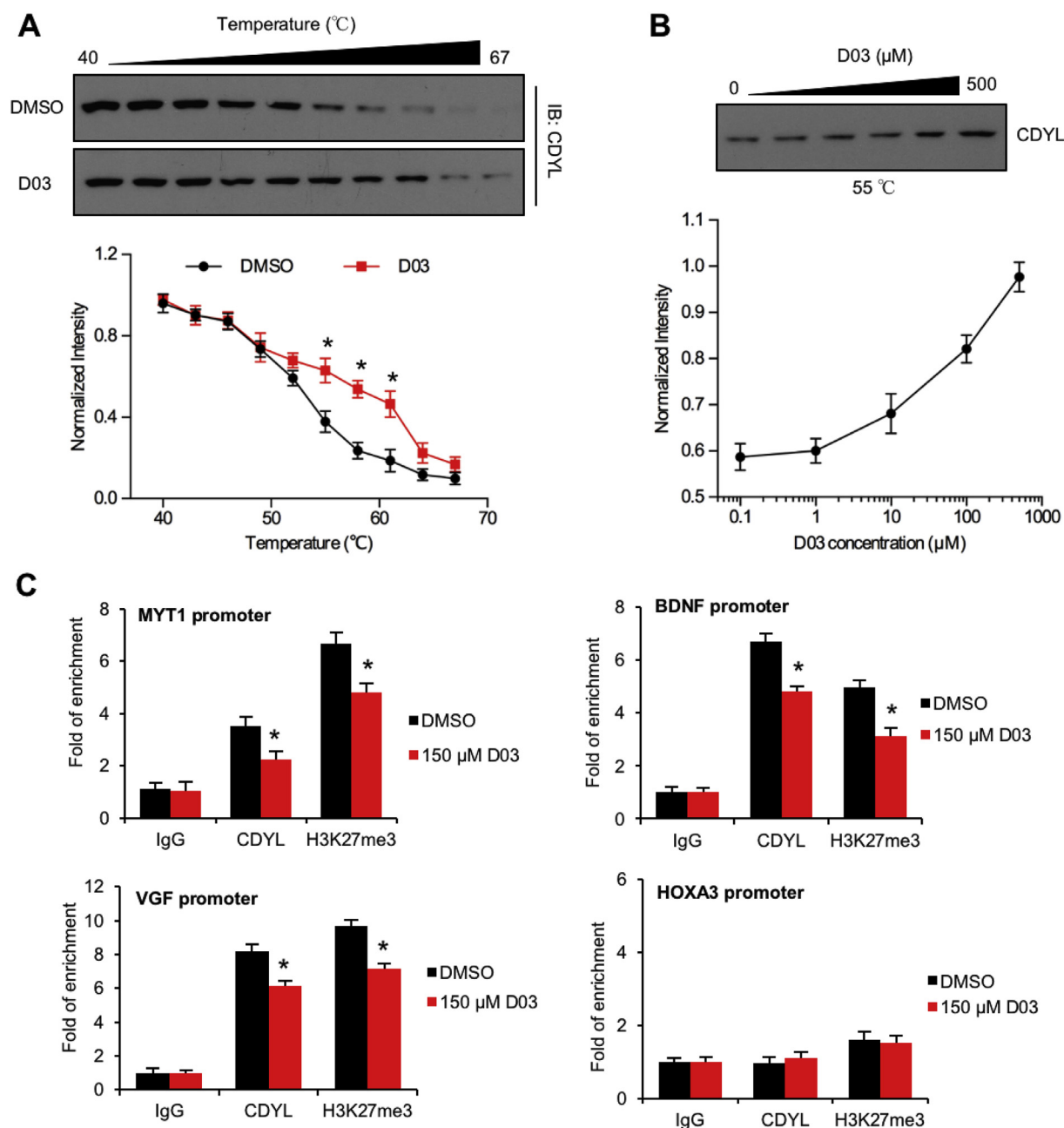


Fig. 5. **D03** perturbs CDYL-chromatin interaction in SH-SY5Y cells. (A) **D03** treatment (150 μM) increases the thermal stability of CDYL in cell lysates as measured by the temperature-dependent cellular thermal shift assay. (B) **D03** treatment increases the thermal stability of CDYL in cell lysates as measured by the concentration-dependent cellular thermal shift assay at 55 °C. (C) ChIP-qPCR analysis of CDYL target genes in SH-SY5Y cells treated with or without **D03** (150 μM) for 24 h. Each bar represents the mean ± S.E.M. for triplicate experiments. *P*-values were determined by Student's *t*-test. **P* < 0.05.

in terms of volumes and interaction types to better fit the hydrophobic cage. Besides, as depicted in Fig. 3B, the benzoxazolone part and molecular flexibility of ligands should be tailored to achieve desired binding preference to CDYL rather than other chromodomains with near-negligible pocket differences.

3. Conclusion

In this study, we explored the possibility of specifically targeting of several chromodomain proteins with high sequence identity by versatile virtual screening technologies, and studied the structure-

activity relationship for small-molecule ligands of CDYL chromodomain. To date, our work was the first successful example to design potent inhibitors of CDYL with the best binding affinity, and some of which like **D03** showed excellent binding preference to the CDYL protein.

However, there are still things we should do to further enhance the affinity and the specificity between CDYL and its inhibitors. As mentioned above, the molecular size and flexibility of the ligands should be well designed to fit the chromodomain of CDYL. Besides, a wider range of reader chromodomains need to be included to better evaluate the selectivity of promising ligands. Moreover, this

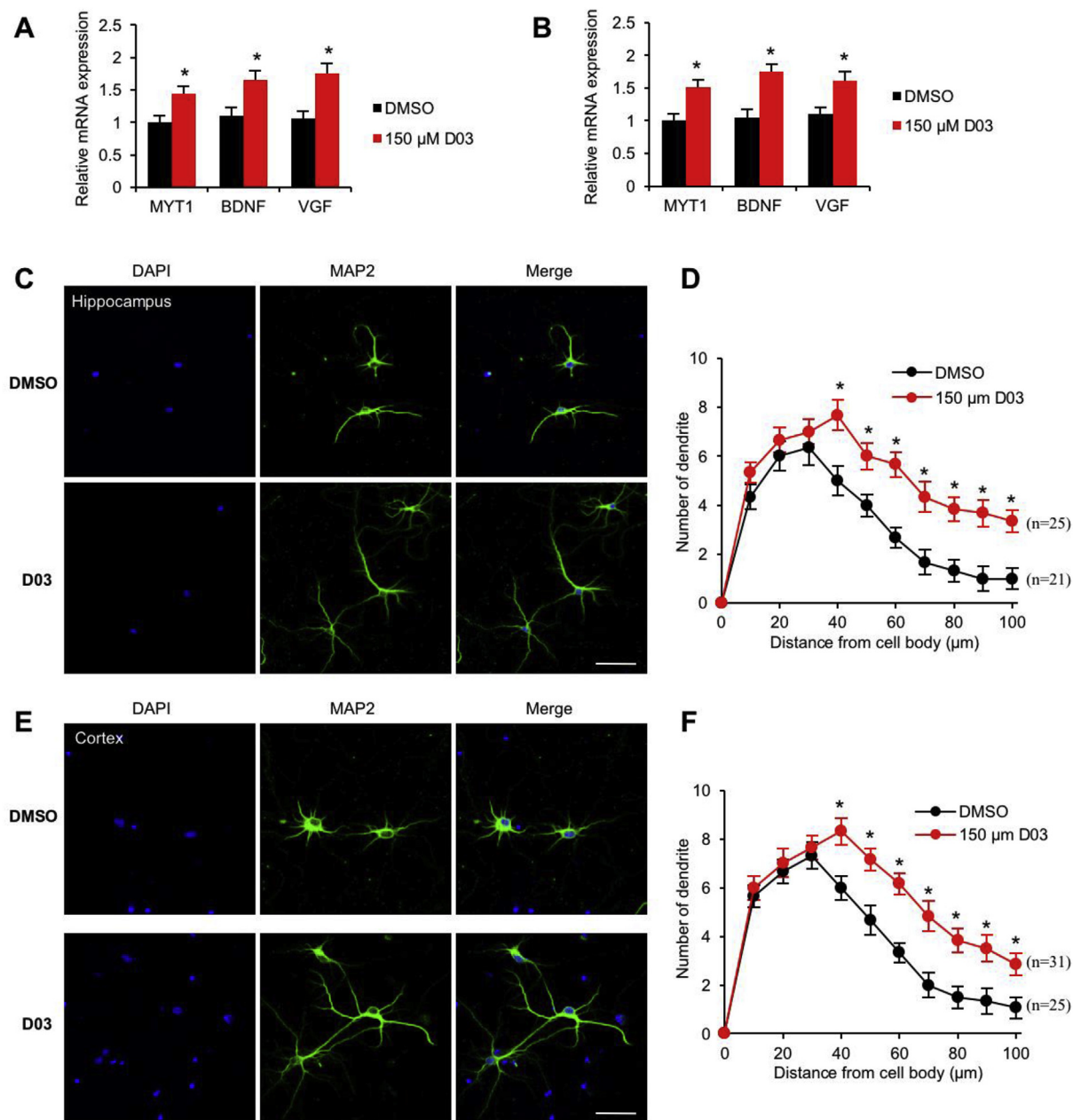


Fig. 6. D03 increases dendritic branching in cultured mouse neurons. RT-qPCR analysis shows mRNA levels of CDYL target genes in mouse hippocampal cells (A) and cortical cells (B) treated with 150 μ M D03 for 24 h. (C, E) Representative images of hippocampal (C) or cortical (E) neurons treated with 150 μ M D03 at DIV 5 (day in vitro) for 24 h. Cells were stained with MAP2 to visualize the morphology of the treated neurons. Scale bar, 50 μ m. (D, F) Sholl analysis of hippocampal (D) or cortical (F) neurons. Each bar represents the mean \pm S.E.M. for triplicate experiments. P -values were determined by Student's t -test. $*P < 0.05$.

study mainly focused on the chemical intervention of CDYL functions in the cellular level, which ignored the therapeutic potential of its inhibitors on neurological diseases. We should give more attentions in the next step to the druggability of CDYL inhibitors, such as their physio-chemical properties which reflect the permeability and stability. In the future, these should be well explored in order to improve the cellular and in vivo efficacy.

In summary, our work on the development of chemical tools for CDYL Kme reader provides the basis for future investigation into the biochemical role of chromodomain-mediated signaling in human diseases.

4. Experimental Section

4.1. Chemistry

Reagents and solvents were purchased from commercial sources and used without further purification. Reaction progress was monitored by UV absorbance using thin-layer chromatography (Silica gel GF254, Qingdao Haiyang Chemical Co., Ltd, Qingdao, China). Silica column chromatography was carried out to purify crude products (Silica gel 200–300 mesh, Shanghai Sanpont Co., Ltd, Shanghai, China). ^1H NMR spectra and ^{13}C NMR spectra were

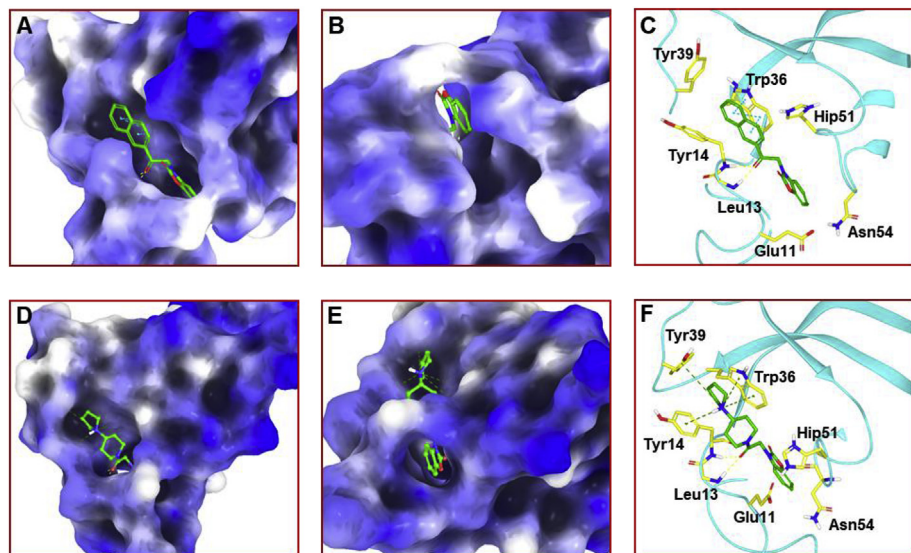


Fig. 7. Induced-fit binding modes for CDYL chromodomain (PDB ID: 2DNT) with **B07** and **D03**. (A) and (B) Local interactions of CDYL with **B07**. (C) The overall docking model of CDYL with **B07**. (D) and (E) Local interactions of CDYL with **D03**. (F) The overall docking model of CDYL with **D03**.

obtained using a Bruker Avance III spectrometer at 400 MHz (Bruker CO., Switzerland) in CDCl_3 or $\text{DMSO}-d_6$ solution with tetramethylsilane as internal standard and chemical shift values were given in ppm. The NMR data was processed by software MestReNova (Version 6.1.0, mestrelab research S.L.), and spectral data were reported using the following abbreviations: (s = singlet, d = doublet, t = triplet, q = quartet, m = multiplet, dd = doublet of doublets); coupling constants are reported in hertz, followed by integration. The high resolution mass (HRMS) was measured on FT-MS-Bruker APEX IV mass spectrometer. Purity of final compounds was determined by RP-HPLC to be >95% (UV detection ($\lambda = 254 \text{ nm}$) and ELSD) using Waters Xbridge C18 column ($4.6 \times 250 \text{ mm } 5 \mu\text{m}$ i.d.). H_2O and MeCN were used as eluents (A is water, B is MeCN). Flow rate was 0.75 mL/min , rt.

4.2. General procedure 1 for the synthesis of compounds **B01–B29**, **C01–C03**

To a stirred suspension of benzo [d]oxazol-2(3H)-one derivative, or benzimidazole, or 2H-benzo [b] [1,4]oxazin-3(4H)-one (1.0 mmol), anhydrous K_2CO_3 (1.2 mmol) was added in the DMF solvent for 20 min at 70°C . Then bromoacetylated **1a–1f** or **2a–2c** (1.3 mmol) and TBAI (0.1 mmol) were added simultaneously. The reaction was stirred and heated for 4 h. After completion, the mixture was extracted with EtOAc/ H_2O three times. The combined organic layers were washed with brine, dried over anhydrous Na_2SO_4 , filtered and concentrated under reduced pressure. The crude product was purified by silica gel column chromatography eluting with EtOAc/PE (3:1–8:1) to afford compounds **B01–B29**, **C01–C03**.

4.3. General procedure 2 for the synthesis of compounds **D01–D08**

To a stirred suspension of benzo [d]oxazol-2(3H)-ones, anhydrous K_2CO_3 (1.2 mmol) was added in the dry DMF solvent for 20 min at 60°C . Then chloroacetylated **3a–3e** (1.3 mmol) and TBAI (0.1 mmol) were added simultaneously. The reaction was stirred and heated for 5 h. After completion, the mixture was extracted with DCM/ H_2O three times. The combined organic layers were washed with brine, dried over anhydrous Na_2SO_4 , filtered and

concentrated under reduced pressure. The crude product was purified by silica gel column chromatography eluting with DCM/ Methanol (20:1–10:1) to afford compounds **D01–D08**.

4.3.1. 5-Chloro-3-hydroxy-3-(2-(3-methoxyphenyl)-2-oxoethyl) indolin-2-one (**AK-778/41314725**)

Off-white solid. Yield: 70%. ^1H NMR (400 MHz, $\text{DMSO}-d_6$) δ 10.38 (s, 1H), 7.50 (d, $J = 7.6 \text{ Hz}$, 1H), 7.46–7.31 (m, 3H), 7.20 (td, $J = 6.9, 5.5, 2.0 \text{ Hz}$, 2H), 6.81 (d, $J = 8.2 \text{ Hz}$, 1H), 6.17 (s, 1H), 4.14 (d, $J = 18.0 \text{ Hz}$, 1H), 3.78 (s, 3H), 3.61 (d, $J = 18.0 \text{ Hz}$, 1H). ^{13}C NMR (101 MHz, $\text{DMSO}-d_6$) δ 196.8, 178.5, 159.8, 142.4, 137.7, 134.4, 130.4, 129.1, 125.6, 124.4, 121.0, 120.22, 112.6, 111.3, 73.5, 55.8, 46.3. HRMS (ESI-TOF $^+$) calcd for $\text{C}_{17}\text{H}_{14}\text{ClNO}_4$ $[\text{M}+\text{H}]^+$ m/z 332.0690, found 332.0691. Commercial source.

4.3.2. (Z)-5-Chloro-3-(2-(3-methoxyphenyl)-2-oxoethylidene) indolin-2-one (**A01**)

To a stirred suspension of **AK-778/41314725** (0.5 mmol), glacial HAc (1.0 mL) and concentrated HCl (50 μL) were added simultaneously in the EtOH solvent. The resulting mixture was heated at 90°C for 1 h. After completion, The red precipitate was filtered and washed with cold EtOH for three times. The crude product was then dried to afford the red solid, **A01**. Yield: 40%. ^1H NMR (400 MHz, $\text{DMSO}-d_6$) δ 10.95 (s, 1H), 8.15 (s, 1H), 7.79 (s, 1H), 7.69 (d, $J = 7.3 \text{ Hz}$, 1H), 7.55 (d, $J = 8.4 \text{ Hz}$, 2H), 7.43 (d, $J = 8.1 \text{ Hz}$, 1H), 7.32 (d, $J = 7.9 \text{ Hz}$, 1H), 6.91 (d, $J = 8.2 \text{ Hz}$, 1H), 3.87 (s, 3H). ^{13}C NMR (101 MHz, $\text{DMSO}-d_6$) δ 191.1, 168.3, 160.2, 144.3, 138.9, 136.4, 132.9, 130.8, 127.5, 126.8, 126.0, 121.9, 121.0, 113.0, 112.3, 55.9. HRMS (ESI-TOF $^+$) calcd for $\text{C}_{17}\text{H}_{12}\text{ClNO}_3$ $[\text{M}+\text{H}]^+$ m/z 314.0584, found 314.0579. HPLC: $t_R = 30.27 \text{ min}$, eluent A-60%, eluent B-40%.

4.3.3. 5-Chloro-3-(2-(3-methoxyphenyl)-2-oxoethyl)indolin-2-one (**A02**)

To the stirred suspension of **A01** (0.5 mmol), Pd/C (0.025 mmol) was added in the anhydrous methanol solvent. The mixture was put in the hydrogen generator under pressure (4 bars) to react overnight in room temperature. After completion, the mixture was filtered and the filtrate was extracted with EtOAc/ H_2O three times. The combined organic layers were washed with brine, dried over anhydrous Na_2SO_4 , filtered and concentrated under reduced

pressure. The crude product was purified by silica gel column chromatography eluting with EtOAc/PE (1:2) to afford the off-white solid, **A02**. Yield: 90%. ^1H NMR (400 MHz, chloroform-*d*) δ 8.70 (s, 1H), 7.58–7.48 (m, 2H), 7.38 (t, *J* = 7.9 Hz, 1H), 7.21 (s, 1H), 7.16 (dd, *J* = 16.8, 8.3 Hz, 2H), 6.84 (d, *J* = 8.2 Hz, 1H), 4.04 (d, *J* = 7.3 Hz, 1H), 3.85 (s, 3H), 3.84–3.78 (m, 1H), 3.49 (dd, *J* = 18.4, 8.4 Hz, 1H). ^{13}C NMR (101 MHz, chloroform-*d*) δ 196.3, 179.8, 159.9, 140.0, 137.3, 131.3, 129.7, 128.1, 127.9, 125.0, 120.8, 120.4, 112.2, 110.7, 55.5, 41.8, 39.7. HRMS (ESI-TOF⁺) calcd for $\text{C}_{17}\text{H}_{14}\text{ClNO}_3$ [$\text{M}+\text{H}$]⁺ *m/z* 316.0740, found 316.0741. HPLC: *t*_R = 30.28 min, eluent A-60%, eluent B-40%.

4.3.4. 6-Chloro-1-(2-(3-methoxyphenyl)-2-oxoethyl)-1,3-dihydro-2H-benzo[d]imidazole-2-one (**A03**)

To the stirred suspension of 5-chloro-1,3-dihydro-2H-benzo [d] imidazole-2-one (1.0 mmol), anhydrous K_2CO_3 (1.0 mmol) was added in the dry CH_3CN solvent for 10 min. Then Boc_2O was added dropwise and reacted for 4 h at 40 °C. After completion, the mixture was extracted with DCM/ H_2O and the combined organic layers were washed, dried. The crude intermediate was purified by silica gel column chromatography eluting with EtOAc/PE (2:3). Then the mono-boc form **A03** was produced following the general procedure 1 (EtOAc/PE = 1:3). At last, the boc group was removed by concentrated HCl in THF at room temperature to afford the off-white solid, **A03**. Yield: 30%. ^1H NMR (400 MHz, DMSO-*d*₆) δ 11.11 (s, 1H), 7.68 (d, *J* = 7.6 Hz, 1H), 7.52 (dd, *J* = 15.8, 7.8 Hz, 2H), 7.29 (d, *J* = 8.9 Hz, 2H), 7.02 (d, *J* = 13.8 Hz, 2H), 5.44 (s, 2H), 3.84 (s, 3H). ^{13}C NMR (101 MHz, DMSO-*d*₆) δ 197.4, 179.0, 159.8, 142.5, 137.8, 132.6, 130.4, 127.6, 125.4, 124.1, 121.0, 120.1, 112.8, 110.7, 55.8, 41.9. HRMS (ESI-TOF⁺) calcd for $\text{C}_{16}\text{H}_{13}\text{ClN}_2\text{O}_3$ [$\text{M}+\text{H}$]⁺ *m/z* 317.0693, found 317.1167. HPLC: *t*_R = 30.20 min, eluent A-60%, eluent B-40%.

4.3.5. 3-(2-(3-Methoxyphenyl)-2-oxoethyl)benzo[d]oxazol-2(3H)-one (**B01**)

Off-white solid. Yield: 80%. ^1H NMR (400 MHz, chloroform-*d*) δ 7.61 (d, *J* = 7.6 Hz, 1H), 7.53 (s, 1H), 7.45 (t, *J* = 7.9 Hz, 1H), 7.24 (d, *J* = 3.3 Hz, 1H), 7.20 (dd, *J* = 8.2, 2.3 Hz, 1H), 7.18–7.10 (m, 2H), 6.86–6.80 (m, 1H), 5.22 (s, 2H), 3.87 (s, 3H). ^{13}C NMR (101 MHz, chloroform-*d*) δ 190.7, 160.0, 142.8, 135.4, 131.1, 130.1, 124.0, 122.8, 121.0, 120.6, 112.3, 110.2, 108.6, 55.5, 48.1. HRMS (ESI-TOF⁺) calcd for $\text{C}_{16}\text{H}_{13}\text{NO}_4$ [$\text{M}+\text{H}$]⁺ *m/z* 284.0923, found 284.0922. HPLC: *t*_R = 26.31 min, eluent A-60%, eluent B-40%.

4.3.6. 5-Fluoro-3-(2-(3-methoxyphenyl)-2-oxoethyl)benzo[d]oxazol-2(3H)-one (**B02**)

Off-white solid. Yield: 80%. ^1H NMR (400 MHz, chloroform-*d*) δ 7.59 (d, *J* = 7.6 Hz, 1H), 7.51 (s, 1H), 7.44 (t, *J* = 7.9 Hz, 1H), 7.18 (ddd, *J* = 16.8, 8.5, 3.1 Hz, 2H), 6.82 (td, *J* = 9.3, 2.4 Hz, 1H), 6.59 (dd, *J* = 7.7, 2.4 Hz, 1H), 5.20 (s, 2H), 3.86 (s, 3H). ^{13}C NMR (101 MHz, chloroform-*d*) δ 190.3, 160.1, 158.3, 154.9, 138.6, 135.2, 132.0, 130.1, 121.1, 120.6, 112.4, 110.8, 109.1, 108.9, 55.5, 48.2. HRMS (ESI-TOF⁺) calcd for $\text{C}_{16}\text{H}_{12}\text{FNO}_4$ [$\text{M}+\text{H}$]⁺ *m/z* 302.0829, found 302.0811. HPLC: *t*_R = 26.04 min, eluent A-60%, eluent B-40%.

4.3.7. 5-Methoxy-3-(2-(3-methoxyphenyl)-2-oxoethyl)benzo[d]oxazol-2(3H)-one (**B03**)

Off-white solid. Yield: 85%. ^1H NMR (400 MHz, chloroform-*d*) δ 7.61 (d, *J* = 7.7 Hz, 1H), 7.53 (s, 1H), 7.45 (t, *J* = 8.0 Hz, 1H), 7.20 (dd, *J* = 8.1, 2.3 Hz, 1H), 7.13 (d, *J* = 8.8 Hz, 1H), 6.63 (dd, *J* = 8.8, 2.5 Hz, 1H), 6.39 (d, *J* = 2.5 Hz, 1H), 5.19 (s, 2H), 3.87 (s, 3H), 3.77 (s, 3H). ^{13}C NMR (101 MHz, chloroform-*d*) δ 190.6, 160.1, 156.8, 155.0, 136.9, 135.4, 131.9, 130.1, 121.0, 120.6, 112.4, 110.4, 107.2, 96.0, 56.0, 55.5, 48.2. HRMS (ESI-TOF⁺) calcd for $\text{C}_{17}\text{H}_{15}\text{NO}_5$ [$\text{M}+\text{H}$]⁺ *m/z* 314.1027, found 314.1028. HPLC: *t*_R = 26.00 min, eluent A-60%, eluent B-40%.

4.3.8. 3-(2-(3-Methoxyphenyl)-2-oxoethyl)-2-oxo-2,3-dihydrobenzo[d]oxazole-5-carbonitrile (**B04**)

Off-white solid. Yield: 60%. ^1H NMR (400 MHz, chloroform-*d*) δ 7.60 (d, *J* = 7.3 Hz, 1H), 7.53–7.50 (m, 1H), 7.49 (dd, *J* = 4.8, 3.2 Hz, 1H), 7.34 (dd, *J* = 8.1, 5.7 Hz, 1H), 7.24 (d, *J* = 7.4 Hz, 2H), 7.09 (s, 1H), 5.26 (s, 2H), 3.88 (s, 3H). ^{13}C NMR (101 MHz, chloroform-*d*) δ 189.8, 160.2, 153.8, 145.5, 135.0, 128.0, 121.4, 120.6, 118.1, 112.4, 112.1, 111.1, 108.0, 55.6, 48.3. HRMS (ESI-TOF⁺) calcd for $\text{C}_{17}\text{H}_{12}\text{N}_2\text{O}_4$ [$\text{M} - \text{H}$][−] *m/z* 304.0719, found 307.0721. HPLC: *t*_R = 5.91 min, eluent A-60%, eluent B-40%.

4.3.9. 3-(2-(3,4-Dimethoxyphenyl)-2-oxoethyl)benzo[d]oxazol-2(3H)-one (**B05**)

Off-white solid. Yield: 90%. ^1H NMR (400 MHz, chloroform-*d*) δ 7.69 (d, *J* = 8.3 Hz, 1H), 7.54 (s, 1H), 7.23 (s, 1H), 7.18–7.09 (m, 2H), 6.95 (d, *J* = 8.4 Hz, 1H), 6.89–6.83 (m, 1H), 5.20 (s, 2H), 3.98 (s, 3H), 3.93 (s, 3H). ^{13}C NMR (101 MHz, chloroform-*d*) δ 189.4, 154.7, 154.4, 149.4, 142.7, 131.2, 127.3, 124.0, 122.9, 122.7, 110.3, 110.2, 108.8, 56.2, 47.7. HRMS (ESI-TOF⁺) calcd for $\text{C}_{17}\text{H}_{15}\text{NO}_5$ [$\text{M}+\text{H}$]⁺ *m/z* 314.1028, found 314.1027. HPLC: *t*_R = 4.04 min, eluent A-30%, eluent B-70%.

4.3.10. 3-(2-(4-(Dimethylamino)phenyl)-2-oxoethyl)benzo[d]oxazol-2(3H)-one (**B06**)

Grey solid. Yield: 85%. ^1H NMR (400 MHz, chloroform-*d*) δ 7.92 (d, *J* = 8.8 Hz, 2H), 7.24–7.19 (m, 1H), 7.11 (p, *J* = 7.1 Hz, 2H), 6.89–6.83 (m, 1H), 6.68 (d, *J* = 8.9 Hz, 2H), 5.14 (s, 2H), 3.09 (s, 6H). ^{13}C NMR (101 MHz, chloroform-*d*) δ 188.2, 154.8, 154.0, 142.7, 131.5, 130.4, 123.9, 122.5, 121.9, 110.8, 110.0, 109.0, 47.4, 40.0. HRMS (ESI-TOF⁺) calcd for $\text{C}_{17}\text{H}_{16}\text{N}_2\text{O}_3$ [$\text{M}+\text{H}$]⁺ *m/z* 297.1239, found 297.1238. HPLC: *t*_R = 6.31 min, eluent A-30%, eluent B-70%.

4.3.11. 3-(2-(Naphthalen-2-yl)-2-oxoethyl)benzo[d]oxazol-2(3H)-one (**B07**)

Off-white solid. Yield: 90%. ^1H NMR (400 MHz, chloroform-*d*) δ 8.59 (s, 1H), 8.09–8.00 (m, 2H), 7.94 (dd, *J* = 17.8, 8.3 Hz, 2H), 7.64 (dt, *J* = 22.4, 7.2 Hz, 2H), 7.27 (s, 1H), 7.15 (td, *J* = 6.8, 5.6, 4.0 Hz, 2H), 6.88 (dd, *J* = 5.9, 3.0 Hz, 1H), 5.38 (s, 2H). ^{13}C NMR (101 MHz, chloroform-*d*) δ 190.7, 142.8, 136.1, 132.4, 131.5, 130.2, 129.7, 129.3, 129.1, 127.9, 127.3, 124.0, 123.4, 122.8, 110.3, 108.7, 48.1. HRMS (ESI-TOF⁺) calcd for $\text{C}_{19}\text{H}_{13}\text{NO}_3$ [$\text{M}+\text{H}$]⁺ *m/z* 304.0974, found 304.0973. HPLC: *t*_R = 6.11 min, eluent A-30%, eluent B-70%.

4.3.12. 3-(2-(Naphthalen-1-yl)-2-oxoethyl)benzo[d]oxazol-2(3H)-one (**B08**)

Off-white solid. Yield: 80%. ^1H NMR (400 MHz, chloroform-*d*) δ 8.75 (d, *J* = 8.4 Hz, 1H), 8.14–8.07 (m, 2H), 7.91 (d, *J* = 7.8 Hz, 1H), 7.65–7.55 (m, 3H), 7.25–7.27 (d, *J* = 7.2 Hz, 1H), 7.15 (tt, *J* = 7.7, 6.1 Hz, 2H), 6.93–6.88 (m, 1H), 5.28 (s, 2H). ^{13}C NMR (101 MHz, chloroform-*d*) δ 194.0, 154.8, 142.8, 134.6, 134.1, 131.6, 131.2, 130.4, 128.6, 127.0, 125.6, 124.3, 124.0, 122.8, 110.3, 108.5, 49.7. HRMS (ESI-TOF⁺) calcd for $\text{C}_{19}\text{H}_{13}\text{NO}_3$ [$\text{M}+\text{H}$]⁺ *m/z* 304.0974, found 304.0975. HPLC: *t*_R = 21.10 min, eluent A-60%, eluent B-40%.

4.3.13. 3-(2-(1H-indol-3-yl)-2-oxoethyl)benzo[d]oxazol-2(3H)-one (**B09**)

Off-white solid. Yield: 70%. ^1H NMR (400 MHz, DMSO-*d*₆) δ 12.24 (s, 1H), 8.61 (s, 1H), 8.07 (d, *J* = 7.6 Hz, 1H), 7.52 (d, *J* = 7.9 Hz, 1H), 7.39 (d, *J* = 7.4 Hz, 1H), 7.19 (dt, *J* = 16.2, 10.0 Hz, 5H), 5.35 (s, 2H). ^{13}C NMR (101 MHz, DMSO-*d*₆) δ 186.8, 154.8, 142.5, 137.0, 135.2, 132.3, 125.7, 124.4, 123.6, 122.7, 122.6, 121.4, 113.9, 112.8, 110.1, 109.9, 48.1. HRMS (ESI-TOF⁺) calcd for $\text{C}_{17}\text{H}_{12}\text{N}_2\text{O}_3$ [$\text{M}+\text{H}$]⁺ *m/z* 293.0926, found 293.0921. HPLC: *t*_R = 4.35 min, eluent A-30%, eluent B-70%.

4.3.14. 3-(2-(3,4-Dimethoxyphenyl)-2-oxoethyl)-5-fluorobenzo[d]oxazol-2(3H)-one (B10)

Off-white solid. Yield: 90%. ^1H NMR (400 MHz, chloroform-*d*) δ 7.66 (d, *J* = 8.2 Hz, 1H), 7.52 (s, 1H), 7.16 (dd, *J* = 8.6, 4.0 Hz, 1H), 6.94 (d, *J* = 8.4 Hz, 1H), 6.81 (t, *J* = 8.8 Hz, 1H), 6.62 (d, *J* = 6.2 Hz, 1H), 5.18 (s, 2H), 3.97 (s, 3H), 3.93 (s, 3H). ^{13}C NMR (101 MHz, chloroform-*d*) δ 189.0, 160.7, 158.3, 155.0, 154.5, 149.5, 138.6, 131.9, 127.1, 123.0, 110.7, 110.1, 109.1, 108.8, 97.7, 56.1, 47.8. HRMS (ESI-TOF $^+$) calcd for $\text{C}_{17}\text{H}_{14}\text{FNO}_5$ [$\text{M}+\text{H}$] $^+$ *m/z* 332.0934, found 332.0932. HPLC:*t*_R = 7.19 min, eluent A-30%, eluent B-70%.

4.3.15. 3-(2-(4-(Dimethylamino)phenyl)-2-oxoethyl)-5-fluorobenzo[d]oxazol-2(3H)-one (B11)

Grey solid. Yield: 65%. ^1H NMR (400 MHz, chloroform-*d*) δ 7.91 (d, *J* = 8.9 Hz, 2H), 7.15 (dd, *J* = 8.7, 4.1 Hz, 1H), 6.80 (td, *J* = 9.2, 2.3 Hz, 1H), 6.69 (d, *J* = 8.9 Hz, 2H), 6.62 (dd, *J* = 7.7, 2.3 Hz, 1H), 5.13 (s, 2H), 3.10 (s, 6H). ^{13}C NMR (101 MHz, chloroform-*d*) δ 187.8, 160.7, 158.3, 155.1, 154.1, 138.6, 132.3, 130.5, 121.7, 110.9, 110.5, 108.8, 108.6, 97.8, 97.5, 47.5, 40.0. HRMS (ESI-TOF $^+$) calcd for $\text{C}_{17}\text{H}_{15}\text{FN}_2\text{O}_3$ [$\text{M}+\text{H}$] $^+$ *m/z* 315.1145, found 315.1132. HPLC:*t*_R = 5.34 min, eluent A-30%, eluent B-70%.

4.3.16. 5-Fluoro-3-(2-(naphthalen-2-yl)-2-oxoethyl)benzo[d]oxazol-2(3H)-one (B12)

Off-white solid. Yield: 86%. ^1H NMR (400 MHz, chloroform-*d*) δ 8.58 (s, 1H), 8.07–7.90 (m, 4H), 7.65 (dt, *J* = 23.0, 7.1 Hz, 2H), 7.19 (dd, *J* = 8.8, 4.1 Hz, 1H), 6.84 (td, *J* = 9.2, 2.5 Hz, 1H), 6.64 (dd, *J* = 7.7, 2.5 Hz, 1H), 5.37 (s, 2H). ^{13}C NMR (101 MHz, chloroform-*d*) δ 190.4, 160.7, 155.0, 136.2, 132.4, 131.3, 130.3, 129.7, 129.4, 129.2, 128.0, 127.3, 123.3, 110.8, 109.1, 108.9, 97.6, 97.3, 48.2. HRMS (ESI-TOF $^+$) calcd for $\text{C}_{19}\text{H}_{12}\text{FNO}_3$ [$\text{M}+\text{H}$] $^+$ *m/z* 322.0879, found 322.0876. HPLC:*t*_R = 5.31 min, eluent A-30%, eluent B-70%.

4.3.17. 3-(2-(1H-indol-3-yl)-2-oxoethyl)-5-fluorobenzo[d]oxazol-2(3H)-one (B13)

Off-white solid. Yield: 50%. ^1H NMR (400 MHz, DMSO-*d*₆) δ 12.21 (s, 1H), 8.59 (d, *J* = 2.5 Hz, 1H), 8.07 (d, *J* = 7.6 Hz, 1H), 7.52 (d, *J* = 7.9 Hz, 1H), 7.42 (dd, *J* = 8.8, 4.2 Hz, 1H), 7.31–7.17 (m, 3H), 7.01–6.92 (m, 1H), 5.35 (s, 2H). ^{13}C NMR (101 MHz, DMSO-*d*₆) δ 186.5, 160.5, 158.2, 155.1, 138.6, 136.9, 135.2, 125.7, 123.7, 122.6, 121.5, 113.8, 112.8, 108.8, 108.6, 98.7, 98.4, 48.3. HRMS (ESI-TOF $^+$) calcd for $\text{C}_{17}\text{H}_{11}\text{FN}_2\text{O}_3$ [$\text{M}+\text{H}$] $^+$ *m/z* 311.0833, found 311.0833. HPLC:*t*_R = 24.27 min, eluent A-60%, eluent B-40%.

4.3.18. 3-(2-(3,4-Dimethoxyphenyl)-2-oxoethyl)-5-methoxybenzo[d]oxazol-2(3H)-one (B14)

Off-white solid. Yield: 95%. ^1H NMR (400 MHz, chloroform-*d*) δ 7.68 (dd, *J* = 8.4, 1.6 Hz, 1H), 7.54 (d, *J* = 1.4 Hz, 1H), 7.12 (d, *J* = 8.8 Hz, 1H), 6.95 (d, *J* = 8.4 Hz, 1H), 6.62 (dd, *J* = 8.8, 2.4 Hz, 1H), 6.43 (d, *J* = 2.4 Hz, 1H), 5.16 (s, 2H), 3.97 (s, 3H), 3.93 (s, 3H), 3.76 (s, 3H). ^{13}C NMR (101 MHz, chloroform-*d*) δ 189.4, 156.8, 155.3, 154.3, 149.4, 136.8, 131.9, 127.3, 122.9, 110.4, 107.2, 96.1, 56.2, 56.1, 56.0, 47.8. HRMS (ESI-TOF $^+$) calcd for $\text{C}_{18}\text{H}_{17}\text{NO}_6$ [$\text{M}+\text{H}$] $^+$ *m/z* 344.1132, found 344.1134. HPLC:*t*_R = 24.37 min, eluent A-60%, eluent B-40%.

4.3.19. 3-(2-(4-(Dimethylamino)phenyl)-2-oxoethyl)-5-methoxybenzo[d]oxazol-2(3H)-one (B15)

Off-white solid. Yield: 87%. ^1H NMR (400 MHz, chloroform-*d*) δ 7.92 (d, *J* = 8.8 Hz, 2H), 7.10 (d, *J* = 8.8 Hz, 1H), 6.68 (d, *J* = 8.9 Hz, 2H), 6.60 (dd, *J* = 8.7, 2.3 Hz, 1H), 6.43 (d, *J* = 2.2 Hz, 1H), 5.11 (s, 2H), 3.75 (s, 3H), 3.09 (s, 6H). ^{13}C NMR (101 MHz, chloroform-*d*) δ 188.2, 156.8, 155.4, 154.0, 136.8, 132.2, 130.5, 121.9, 110.8, 110.2, 107.2, 96.1, 56.0, 47.4, 40.0. HRMS (ESI-TOF $^+$) calcd for $\text{C}_{18}\text{H}_{18}\text{N}_2\text{O}_4$ [$\text{M}+\text{H}$] $^+$ *m/z* 327.1245, found 327.1243. HPLC:*t*_R = 4.31 min, eluent A-30%, eluent B-70%.

4.3.20. 5-Methoxy-3-(2-(naphthalen-2-yl)-2-oxoethyl)benzo[d]oxazol-2(3H)-one (B16)

Off-white solid. Yield: 80%. ^1H NMR (400 MHz, chloroform-*d*) δ 8.58 (s, 1H), 8.02 (t, *J* = 9.8 Hz, 2H), 7.93 (dd, *J* = 15.7, 8.4 Hz, 2H), 7.63 (dt, *J* = 22.8, 7.0 Hz, 2H), 7.13 (d, *J* = 8.8 Hz, 1H), 6.63 (dd, *J* = 8.8, 2.2 Hz, 1H), 6.44 (d, *J* = 2.2 Hz, 1H), 5.34 (s, 2H), 3.76 (s, 3H). ^{13}C NMR (101 MHz, chloroform-*d*) δ 190.7, 156.8, 155.3, 136.9, 136.1, 132.4, 131.9, 131.5, 130.3, 129.7, 129.2, 129.1, 127.9, 127.3, 123.4, 110.4, 107.3, 96.0, 56.0, 48.1. HRMS (ESI-TOF $^+$) calcd for $\text{C}_{20}\text{H}_{15}\text{NO}_4$ [$\text{M}+\text{H}$] $^+$ *m/z* 334.1079, found 334.1082. HPLC:*t*_R = 21.89 min, eluent A-60%, eluent B-40%.

4.3.21. 3-(2-(1H-indol-3-yl)-2-oxoethyl)-5-methoxybenzo[d]oxazol-2(3H)-one (B17)

Off-white solid. Yield: 60%. ^1H NMR (400 MHz, DMSO-*d*₆) δ 12.20 (s, 1H), 8.59 (s, 1H), 8.08 (d, *J* = 7.6 Hz, 1H), 7.52 (d, *J* = 7.8 Hz, 1H), 7.31–7.17 (m, 3H), 6.95 (s, 1H), 6.67 (d, *J* = 8.6 Hz, 1H), 5.34 (s, 2H), 3.71 (s, 3H). ^{13}C NMR (101 MHz, DMSO-*d*₆) δ 186.8, 156.9, 155.4, 136.9, 136.5, 135.1, 125.7, 123.6, 122.6, 121.5, 113.9, 112.8, 110.5, 107.7, 96.7, 56.3, 48.1. HRMS (ESI-TOF $^+$) calcd for $\text{C}_{18}\text{H}_{14}\text{N}_2\text{O}_4$ [$\text{M}+\text{H}$] $^+$ *m/z* 323.1032, found 323.1026. HPLC:*t*_R = 23.67 min, eluent A-60%, eluent B-40%.

4.3.22. 5-Bromo-3-(2-(naphthalen-2-yl)-2-oxoethyl)benzo[d]oxazol-2(3H)-one (B18)

Brown solid. Yield: 90%. ^1H NMR (400 MHz, chloroform-*d*) δ 8.58 (s, 1H), 7.99 (ddd, *J* = 27.8, 18.4, 8.5 Hz, 4H), 7.65 (dt, *J* = 23.1, 6.9 Hz, 2H), 7.29 (d, *J* = 1.9 Hz, 1H), 7.14 (d, *J* = 8.5 Hz, 1H), 7.01 (d, *J* = 1.8 Hz, 1H), 5.36 (s, 2H). ^{13}C NMR (101 MHz, chloroform-*d*) δ 190.2, 154.3, 141.8, 136.2, 132.5, 132.4, 131.3, 130.3, 129.7, 129.4, 129.2, 128.0, 128.0, 127.4, 125.7, 123.3, 116.6, 112.0, 111.5, 48.2. HRMS (ESI-TOF $^+$) calcd for $\text{C}_{19}\text{H}_{12}\text{BrNO}_3$ [$\text{M}+\text{H}$] $^+$ *m/z* 382.0079, found 382.0078. HPLC:*t*_R = 23.52 min, eluent A-60%, eluent B-40%.

4.3.23. 3-(2-(Naphthalen-2-yl)-2-oxoethyl)-2-oxo-2,3-dihydrobenzo[d]oxazole-5-carbonitrile (B19)

Off-white solid. Yield: 40%. ^1H NMR (400 MHz, chloroform-*d*) δ 8.57 (s, 1H), 8.06–7.89 (m, 4H), 7.66 (dt, *J* = 23.7, 7.1 Hz, 2H), 7.49 (d, *J* = 7.3 Hz, 1H), 7.34 (d, *J* = 8.3 Hz, 1H), 7.15 (s, 1H), 5.42 (s, 2H). ^{13}C NMR (101 MHz, chloroform-*d*) δ 189.9, 153.8, 145.5, 136.2, 132.4, 132.0, 131.1, 130.4, 129.7, 129.5, 129.3, 128.0, 127.4, 123.2, 118.2, 112.2, 111.0, 108.0, 48.3. HRMS (ESI-TOF $^+$) calcd for $\text{C}_{20}\text{H}_{12}\text{N}_2\text{O}_3$ [$\text{M}+\text{H}$] $^+$ *m/z* 329.0926, found 329.0925. HPLC:*t*_R = 26.06 min, eluent A-60%, eluent B-40%.

4.3.24. 6-Bromo-3-(2-(naphthalen-2-yl)-2-oxoethyl)benzo[d]oxazol-2(3H)-one (B20)

Light yellow solid. Yield: 90%. ^1H NMR (400 MHz, chloroform-*d*) δ 8.57 (s, 1H), 7.98 (dd, *J* = 16.9, 9.1 Hz, 4H), 7.65 (dt, *J* = 22.1, 6.9 Hz, 2H), 7.43 (d, *J* = 1.7 Hz, 1H), 7.30 (dd, *J* = 8.3, 1.7 Hz, 1H), 6.75 (d, *J* = 8.3 Hz, 1H), 5.37 (s, 2H). ^{13}C NMR (101 MHz, chloroform-*d*) δ 190.2, 154.3, 141.8, 136.2, 132.5, 132.4, 131.3, 130.3, 129.7, 129.4, 129.2, 128.0, 127.4, 125.7, 123.3, 116.62, 112.0, 111.5, 48.2. HRMS (ESI-TOF $^+$) calcd for $\text{C}_{19}\text{H}_{12}\text{BrNO}_3$ [$\text{M}+\text{H}$] $^+$ *m/z* 382.0079, found 382.0081. HPLC:*t*_R = 23.19 min, eluent A-60%, eluent B-40%.

4.3.25. 6-Amino-3-(2-(naphthalen-2-yl)-2-oxoethyl)benzo[d]thiazol-2(3H)-one (B21)

Off-white solid. Yield: 20%. ^1H NMR (400 MHz, DMSO-*d*₆) δ 8.89 (s, 1H), 8.17 (s, 2H), 8.05 (dt, *J* = 17.1, 8.7 Hz, 4H), 6.96 (d, *J* = 8.7 Hz, 1H), 6.82 (d, *J* = 1.8 Hz, 1H), 6.53 (d, *J* = 10.4 Hz, 1H), 5.65 (s, 2H), 5.05 (s, 2H). ^{13}C NMR (101 MHz, DMSO-*d*₆) δ 192.9, 168.9, 145.9, 135.9, 132.5, 132.1, 131.1, 130.1, 129.6, 129.0, 128.3, 128.0, 127.7, 123.8, 122.4, 113.3, 112.4, 107.7, 49.3. HRMS (ESI-TOF $^+$) calcd for $\text{C}_{19}\text{H}_{14}\text{N}_2\text{O}_2\text{S}$ [$\text{M}+\text{H}$] $^+$ *m/z* 335.0854, found 335.0851.

HPLC: t_R = 19.12 min, eluent A-60%, eluent B-40%.

4.3.26. 3-(2-(Naphthalen-2-yl)-2-oxoethyl)-6-nitrobenzo[d]thiazol-2(3H)-one (**B22**)

Yellow solid. Yield: 70%. ^1H NMR (400 MHz, chloroform- d_6) δ 8.60 (s, 1H), 8.41 (d, J = 2.3 Hz, 1H), 8.19 (dd, J = 8.9, 2.3 Hz, 1H), 8.06–7.90 (m, 4H), 7.66 (dt, J = 22.3, 7.5 Hz, 2H), 6.96 (d, J = 8.9 Hz, 1H), 5.59 (s, 2H). ^{13}C NMR (101 MHz, chloroform- d_6) δ 190.0, 169.9, 143.7, 141.9, 136.2, 132.4, 131.3, 130.3, 129.7, 129.5, 129.3, 128.0, 127.4, 123.4, 123.3, 122.8, 118.8, 110.4, 48.9. HRMS (ESI-TOF $^+$) calcd for $\text{C}_{19}\text{H}_{12}\text{N}_2\text{O}_4\text{S}$ $[\text{M} - \text{H}]^-$ m/z 363.0440, found 363.0439. HPLC: t_R = 25.06 min, eluent A-60%, eluent B-40%.

4.3.27. 3-(2-(1H-indol-3-yl)-2-oxoethyl)-2-oxo-2,3-dihydrobenzo[d]oxazole-5-carbonitrile (**B23**)

Off-white solid. Yield: 30%. ^1H NMR (400 MHz, DMSO- d_6) δ 12.23 (s, 1H), 8.60 (s, 1H), 8.07 (d, J = 7.6 Hz, 1H), 7.88 (s, 1H), 7.71–7.60 (m, 2H), 7.53 (d, J = 7.9 Hz, 1H), 7.22 (dt, J = 20.1, 7.1 Hz, 2H), 5.40 (s, 2H). ^{13}C NMR (101 MHz, DMSO- d_6) δ 186.3, 154.3, 145.5, 136.9, 135.3, 133.3, 128.2, 125.7, 123.7, 122.7, 121.4, 119.0, 113.7, 113.5, 112.8, 111.4, 107.0, 48.4. HRMS (ESI-TOF $^+$) calcd for $\text{C}_{18}\text{H}_{11}\text{N}_3\text{O}_3$ $[\text{M} + \text{H}]^+$ m/z 318.0879, found 318.0882. HPLC: t_R = 25.10 min, eluent A-60%, eluent B-40%.

4.3.28. 3-(2-(1H-indol-3-yl)-2-oxoethyl)-6-aminobenzo[d]thiazol-2(3H)-one (**B24**)

Light yellow solid. Yield: 60%. ^1H NMR (400 MHz, DMSO- d_6) δ 12.16 (s, 1H), 8.61 (s, 1H), 8.08 (d, J = 7.5 Hz, 1H), 7.51 (d, J = 8.0 Hz, 1H), 7.21 (dt, J = 19.7, 7.1 Hz, 2H), 6.86 (d, J = 8.6 Hz, 1H), 6.81 (d, J = 2.1 Hz, 1H), 6.52 (dd, J = 8.6, 2.1 Hz, 1H), 5.30 (s, 2H), 5.01 (s, 2H). ^{13}C NMR (101 MHz, DMSO- d_6) δ 187.2, 168.9, 145.8, 136.9, 135.0, 128.3, 125.7, 123.6, 122.6, 122.4, 121.5, 114.1, 113.2, 112.8, 112.3, 107.7, 48.7. HRMS (ESI-TOF $^+$) calcd for $\text{C}_{17}\text{H}_{13}\text{N}_3\text{O}_2\text{S}$ $[\text{M} + \text{H}]^+$ m/z 324.0807, found 324.0801. HPLC: t_R = 25.22 min, eluent A-60%, eluent B-40%.

4.3.29. 3-(2-(1H-indol-3-yl)-2-oxoethyl)-6-nitrobenzo[d]thiazol-2(3H)-one (**B25**)

Yellow solid. Yield: 50%. ^1H NMR (400 MHz, DMSO- d_6) δ 12.24 (s, 1H), 8.79 (d, J = 2.1 Hz, 1H), 8.65 (d, J = 3.0 Hz, 1H), 8.22 (dd, J = 9.0, 2.1 Hz, 1H), 8.05 (d, J = 7.7 Hz, 1H), 7.50 (dd, J = 20.3, 8.5 Hz, 2H), 7.22 (dt, J = 22.1, 7.2 Hz, 2H), 5.58 (s, 2H). ^{13}C NMR (101 MHz, DMSO- d_6) δ 186.2, 170.3, 143.4, 136.9, 135.5, 125.6, 123.7, 123.3, 122.8, 122.7, 121.4, 119.8, 113.9, 112.8, 112.1, 49.3. HRMS (ESI-TOF $^+$) calcd for $\text{C}_{17}\text{H}_{11}\text{N}_3\text{O}_4\text{S}$ $[\text{M} + \text{H}]^+$ m/z 354.0549, found 354.0548. HPLC: t_R = 25.24 min, eluent A-60%, eluent B-40%.

4.3.30. 2-(1H-benzo[d]imidazole-1-yl)-1-(3-methoxyphenyl)ethan-1-one (**B26**)

Off-white solid. Yield: 60%. ^1H NMR (400 MHz, chloroform- d) δ 8.00 (s, 1H), 7.86–7.80 (m, 1H), 7.55 (d, J = 7.6 Hz, 1H), 7.46 (s, 1H), 7.40 (t, J = 7.9 Hz, 1H), 7.23 (d, J = 3.9 Hz, 2H), 7.20–7.14 (m, 2H), 5.51 (s, 2H), 3.80 (s, 3H). ^{13}C NMR (101 MHz, chloroform- d) δ 191.2, 160.1, 144.1, 142.6, 135.4, 134.1, 130.1, 123.6, 123.3, 122.7, 120.9, 120.5, 120.0, 112.4, 109.6, 55.5, 50.7. HRMS (ESI-TOF $^+$) calcd for $\text{C}_{16}\text{H}_{14}\text{N}_2\text{O}_2$ $[\text{M} + \text{H}]^+$ m/z 267.1134, found 267.1132. HPLC: t_R = 7.11 min, eluent A-30%, eluent B-70%.

4.3.31. 4-(2-(3-Methoxyphenyl)-2-oxoethyl)-2H-benzo[b][1,4]oxazin-3(4H)-one (**B27**)

Off-white solid. Yield: 40%. ^1H NMR (400 MHz, chloroform- d) δ 7.62 (d, J = 7.5 Hz, 1H), 7.54 (s, 1H), 7.44 (t, J = 7.9 Hz, 1H), 7.19 (d, J = 8.1 Hz, 1H), 7.00 (q, J = 7.8 Hz, 2H), 6.93 (t, J = 7.5 Hz, 1H), 6.62 (d, J = 7.8 Hz, 1H), 5.33 (s, 2H), 4.72 (s, 2H), 3.86 (s, 3H). ^{13}C NMR (101 MHz, chloroform- d) δ 191.7, 165.1, 160.1, 145.1, 135.8, 130.0,

128.8, 124.1, 122.9, 120.5, 117.1, 114.7, 112.4, 110.0, 67.5, 55.5, 48.0. HRMS (ESI-TOF $^+$) calcd for $\text{C}_{17}\text{H}_{15}\text{NO}_4$ $[\text{M} + \text{H}]^+$ m/z 298.1079, found 298.1081. HPLC: t_R = 19.10 min, eluent A-60%, eluent B-40%.

4.3.32. 4-(2-(Naphthalen-2-yl)-2-oxoethyl)-2H-benzo[b][1,4]oxazin-3(4H)-one (**B28**)

Off-white solid. Yield: 40%. ^1H NMR (400 MHz, chloroform- d) δ 8.58 (s, 1H), 7.98 (dd, J = 18.6, 8.0 Hz, 4H), 7.62 (dd, J = 15.5, 7.4 Hz, 2H), 7.09–6.97 (m, 2H), 6.94 (d, J = 7.0 Hz, 1H), 6.67 (d, J = 7.3 Hz, 1H), 5.48 (s, 2H), 4.75 (s, 2H). ^{13}C NMR (101 MHz, Chloroform- d) δ 191.8, 165.2, 145.2, 136.0, 132.4, 131.9, 130.0, 129.7, 129.1, 129.0, 127.9, 127.2, 124.1, 123.5, 122.9, 117.1, 114.8, 67.6, 48.0. HRMS (ESI-TOF $^+$) calcd for $\text{C}_{20}\text{H}_{15}\text{NO}_3$ $[\text{M} + \text{H}]^+$ m/z 318.1130, found 318.1129. HPLC: t_R = 20.85 min, eluent A-60%, eluent B-40%.

4.3.33. 4-(2-(1H-indol-3-yl)-2-oxoethyl)-2H-benzo[b][1,4]oxazin-3(4H)-one (**B29**)

Off-white solid. Yield: 20%. ^1H NMR (400 MHz, DMSO- d_6) δ 12.16 (s, 1H), 8.62 (d, J = 3.1 Hz, 1H), 8.09 (d, J = 7.6 Hz, 1H), 7.51 (d, J = 8.0 Hz, 1H), 7.21 (dt, J = 20.6, 6.8 Hz, 2H), 7.04 (d, J = 8.0 Hz, 1H), 6.97 (d, J = 15.5 Hz, 3H), 5.36 (s, 2H), 4.74 (s, 2H). ^{13}C NMR (101 MHz, DMSO- d_6) δ 187.6, 165.0, 145.1, 136.9, 134.8, 129.6, 125.8, 123.9, 123.5, 123.1, 122.5, 121.5, 117.0, 115.9, 114.1, 112.8, 67.4, 47.6. HRMS (ESI-TOF $^+$) calcd for $\text{C}_{18}\text{H}_{14}\text{N}_2\text{O}_3$ $[\text{M} + \text{H}]^+$ m/z 305.0026, found 305.0921. HPLC: t_R = 23.73 min, eluent A-60%, eluent B-40%.

4.3.34. N-(3-methoxyphenyl)-2-(2-oxobenzo[d]oxazol-3(2H)-yl)acetamide (**C01**)

Off-white solid. Yield: 70%. ^1H NMR (400 MHz, DMSO- d_6) δ 10.42 (s, 1H), 7.37 (d, J = 7.9 Hz, 1H), 7.28 (dd, J = 4.4, 2.0 Hz, 2H), 7.21 (td, J = 7.8, 3.7 Hz, 2H), 7.18–7.06 (m, 2H), 6.65 (dd, J = 8.2, 1.9 Hz, 1H), 4.71 (s, 2H), 3.70 (s, 3H). ^{13}C NMR (101 MHz, DMSO- d_6) δ 165.2, 159.8, 154.6, 142.4, 140.1, 132.0, 130.2, 124.4, 122.8, 111.9, 110.2, 109.7, 105.3, 55.1, 45.1. HRMS (ESI-TOF $^+$) calcd for $\text{C}_{16}\text{H}_{14}\text{N}_2\text{O}_4$ $[\text{M} + \text{H}]^+$ m/z 299.0561, found 299.0564. HPLC: t_R = 25.19 min, eluent A-60%, eluent B-40%.

4.3.35. N-(naphthalen-2-yl)-2-(2-oxobenzo[d]oxazol-3(2H)-yl)acetamide (**C02**)

Off-white solid. Yield: 75%. ^1H NMR (400 MHz, DMSO- d_6) δ 10.66 (s, 1H), 8.26 (s, 1H), 7.88 (d, J = 8.7 Hz, 1H), 7.84 (d, J = 7.8 Hz, 1H), 7.79 (d, J = 8.3 Hz, 1H), 7.58 (d, J = 8.4 Hz, 1H), 7.50–7.43 (m, 1H), 7.41 (d, J = 7.8 Hz, 2H), 7.32 (d, J = 7.3 Hz, 1H), 7.22 (t, J = 7.4 Hz, 1H), 7.16 (d, J = 7.8 Hz, 1H), 4.79 (s, 2H). ^{13}C NMR (101 MHz, DMSO- d_6) δ 168.7, 149.9, 134.5, 130.6, 129.6, 128.8, 128.6, 127.1, 126.8, 125.4, 125.1, 122.6, 121.8, 121.5, 120.8, 52.0. HRMS (ESI-TOF $^+$) calcd for $\text{C}_{19}\text{H}_{14}\text{N}_2\text{O}_3$ $[\text{M} + \text{H}]^+$ m/z 319.1083, found 319.1087. HPLC: t_R = 21.74 min, eluent A-60%, eluent B-40%.

4.3.36. N-(naphthalen-1-yl)-2-(2-oxobenzo[d]oxazol-3(2H)-yl)acetamide (**C03**)

Off-white solid. Yield: 75%. ^1H NMR (400 MHz, chloroform- d) δ 8.01 (d, J = 8.2 Hz, 1H), 7.99–7.92 (m, 1H), 7.69 (t, J = 9.5 Hz, 2H), 7.63–7.55 (m, 3H), 7.51 (d, J = 7.3 Hz, 1H), 7.23–7.20 (m, 1H), 7.10 (d, J = 8.0 Hz, 1H), 7.04 (t, J = 7.7 Hz, 1H), 4.75 (q, J = 17.7 Hz, 2H). ^{13}C NMR (101 MHz, chloroform- d) δ 168.7, 149.9, 134.5, 128.8, 128.6, 127.5, 126.8, 125.4, 122.6, 121.8, 121.5, 120.8, 52.0. HRMS (ESI-TOF $^+$) calcd for $\text{C}_{19}\text{H}_{14}\text{N}_2\text{O}_3$ $[\text{M} + \text{H}]^+$ m/z 319.1083, found 319.1086. HPLC: t_R = 21.70 min, eluent A-60%, eluent B-40%.

4.3.37. 3-(2-(4-(Dimethylamino)piperidin-1-yl)-2-oxoethyl)benzo[d]oxazol-2(3H)-one (**D01**)

Off-white solid. Yield: 40%. ^1H NMR (400 MHz, DMSO- d_6) δ 7.34 (d, J = 7.7 Hz, 1H), 7.19 (d, J = 0.7 Hz, 1H), 7.19–7.17 (m, 1H), 7.14–7.08 (m, 1H), 4.87–4.73 (m, 2H), 4.33–4.23 (m, 1H), 3.94 (d,

$J = 12.1$ Hz, 1H), 3.19–3.01 (m, 2H), 2.59 (t, $J = 13.8$ Hz, 1H), 2.48 (s, 6H), 1.83–1.68 (m, 2H), 1.41–1.34 (m, 2H). ^{13}C NMR (101 MHz, DMSO- d_6) δ 163.9, 154.7, 142.4, 132.1, 124.2, 110.0, 61.8, 50.1, 44.09, 43.4, 23.5, 14.0. HRMS (ESI-TOF $^+$) calcd for $\text{C}_{16}\text{H}_{21}\text{N}_3\text{O}_3$ $[\text{M}+\text{H}]^+$ m/z 304.1661, found 304.1655. HPLC: $t_R = 23.66$ min, eluent A-60%, eluent B-40%.

4.3.38. 3-(2-(4-(Diethylamino)piperidin-1-yl)-2-oxoethyl)benzo[d]oxazol-2(3H)-one (D02)

Off-white solid. Yield: 45%. ^1H NMR (400 MHz, DMSO- d_6) δ 7.34 (d, $J = 7.7$ Hz, 1H), 7.19 (d, $J = 6.8$ Hz, 2H), 7.13 (q, $J = 8.7$, 7.0 Hz, 1H), 4.81 (q, $J = 17.0$ Hz, 2H), 4.30 (d, $J = 12.3$ Hz, 1H), 3.94 (d, $J = 12.7$ Hz, 1H), 3.08 (t, $J = 12.6$ Hz, 1H), 2.73 (d, $J = 9.0$ Hz, 1H), 2.64–2.56 (m, 1H), 2.49 (s, 4H), 1.79–1.63 (m, 2H), 1.35–1.14 (m, 2H), 0.94 (d, $J = 11.7$ Hz, 6H). ^{13}C NMR (101 MHz, Chloroform- d) δ 163.3, 154.6, 142.6, 131.2, 124.0, 122.9, 110.0, 109.1, 57.6, 43.6, 42.2, 29.1, 27.9, 13.6. HRMS (ESI-TOF $^+$) calcd for $\text{C}_{18}\text{H}_{25}\text{N}_3\text{O}_3$ $[\text{M}+\text{H}]^+$ m/z 332.1974, found 332.1974. HPLC: $t_R = 21.73$ min, eluent A-60%, eluent B-40%.

4.3.39. 3-(2-Oxo-2-(4-(pyrrolidin-1-yl)piperidin-1-yl)ethyl)benzo[d]oxazol-2(3H)-one (D03)

Off-white solid. Yield: 30%. ^1H NMR (400 MHz, chloroform- d) δ 7.21 (d, $J = 6.8$ Hz, 1H), 7.18–7.13 (m, 1H), 7.13–7.08 (m, 1H), 7.00 (d, $J = 7.8$ Hz, 1H), 4.62 (d, $J = 3.1$ Hz, 2H), 4.39 (d, $J = 12.8$ Hz, 1H), 3.90 (s, 1H), 3.20 (t, $J = 11.2$ Hz, 1H), 2.85 (t, $J = 11.0$ Hz, 1H), 2.58 (s, 4H), 2.33–2.22 (m, 1H), 1.96 (dd, $J = 31.8$, 10.5 Hz, 2H), 1.79 (d, $J = 6.4$ Hz, 4H), 1.50 (dd, $J = 18.3$, 11.7 Hz, 2H). ^{13}C NMR (101 MHz, chloroform- d) δ 163.4, 154.6, 142.6, 131.2, 124.0, 122.7, 110.1, 109.3, 61.1, 51.5, 43.7, 41.0, 31.8, 23.2. HRMS (ESI-TOF $^+$) calcd for $\text{C}_{18}\text{H}_{23}\text{N}_3\text{O}_3$ $[\text{M}+\text{H}]^+$ m/z 330.1818, found 330.1814. HPLC: $t_R = 5.27$ min, eluent A-30%, eluent B-70%.

4.3.40. 3-(2-([1,4'-Bipiperidin]-1'-yl)-2-oxoethyl)benzo[d]oxazol-2(3H)-one (D04)

Off-white solid. Yield: 30%. ^1H NMR (400 MHz, DMSO- d_6) δ 7.33 (d, $J = 7.8$ Hz, 1H), 7.21 (t, $J = 6.4$ Hz, 1H), 7.16 (d, $J = 7.5$ Hz, 1H), 7.11 (t, $J = 8.2$ Hz, 1H), 4.82 (q, $J = 17.1$ Hz, 2H), 4.29 (d, $J = 12.9$ Hz, 1H), 3.95 (d, $J = 13.2$ Hz, 1H), 3.21–2.99 (m, 2H), 2.64–2.52 (m, 2H), 1.77 (dd, $J = 27.2$, 12.1 Hz, 2H), 1.57 (s, 3H), 1.42–1.18 (m, 6H), 0.92 (t, $J = 7.3$ Hz, 2H). ^{13}C NMR (101 MHz, DMSO- d_6) δ 163.9, 154.7, 142.4, 132.1, 124.2, 122.6, 110.1, 110.0, 61.8, 50.0, 44.1, 43.4, 41.7, 28.2, 27.5, 26.2, 24.7, 19.7, 14.0. HRMS (ESI-TOF $^+$) calcd for $\text{C}_{19}\text{H}_{25}\text{N}_3\text{O}_3$ $[\text{M}+\text{H}]^+$ m/z 344.1974, found 344.1971. HPLC: $t_R = 23.80$ min, eluent A-60%, eluent B-40%.

4.3.41. 3-(2-(4-Morpholinopiperidin-1-yl)-2-oxoethyl)benzo[d]oxazol-2(3H)-one (D05)

Off-white solid. Yield: 30%. ^1H NMR (400 MHz, chloroform- d) δ 7.21 (d, $J = 7.7$ Hz, 1H), 7.14 (dq, $J = 15.0$, 7.5 Hz, 2H), 7.00 (d, $J = 7.4$ Hz, 1H), 4.70–4.56 (m, 2H), 4.52 (d, $J = 13.1$ Hz, 1H), 3.97 (d, $J = 13.7$ Hz, 1H), 3.75–3.67 (m, 4H), 3.16 (t, $J = 12.1$ Hz, 1H), 2.72 (t, $J = 11.6$ Hz, 1H), 2.56–2.48 (m, 4H), 2.43 (t, $J = 10.9$ Hz, 1H), 2.01–1.57 (m, 4H). ^{13}C NMR (101 MHz, chloroform- d) δ 163.4, 154.6, 142.6, 131.2, 124.0, 122.7, 110.1, 109.2, 67.2, 61.4, 49.8, 44.4, 43.7, 41.6, 28.7, 27.9. HRMS (ESI-TOF $^+$) calcd for $\text{C}_{18}\text{H}_{23}\text{N}_3\text{O}_4$ $[\text{M}+\text{H}]^+$ m/z 346.1767, found 346.1762. HPLC: $t_R = 30.18$ min, eluent A-60%, eluent B-40%.

4.3.42. 3-(2-(4-(Diethylamino)piperidin-1-yl)-2-oxoethyl)-5-fluorobenzo[d]oxazol-2(3H)-one (D06)

Off-white solid. Yield: 25%. ^1H NMR (400 MHz, chloroform- d) δ 7.13 (dd, $J = 8.6$, 3.9 Hz, 1H), 6.81 (d, $J = 9.0$ Hz, 1H), 6.78–6.72 (m, 1H), 4.60 (d, $J = 13.4$ Hz, 2H), 3.92 (d, $J = 13.8$ Hz, 1H), 3.13 (t, $J = 12.7$ Hz, 1H), 2.80 (t, $J = 11.2$ Hz, 1H), 2.66 (d, $J = 12.4$ Hz, 1H), 2.57 (q, $J = 6.9$ Hz, 3H), 1.88 (dd, $J = 35.0$, 12.6 Hz, 2H), 1.49 (dt,

$J = 24.5$, 12.9 Hz, 3H), 1.06 (t, $J = 7.0$ Hz, 6H), 0.92–0.78 (m, 1H). ^{13}C NMR (101 MHz, chloroform- d) δ 163.0, 160.7, 158.1, 153.3, 138.5, 132.1, 110.6, 108.8, 57.6, 44.9, 43.5, 42.2, 29.16, 28.0, 13.5. HRMS (ESI-TOF $^+$) calcd for $\text{C}_{18}\text{H}_{24}\text{FN}_3\text{O}_3$ $[\text{M}+\text{H}]^+$ m/z 350.1880, found 350.1874. HPLC: $t_R = 23.81$ min, eluent A-60%, eluent B-40%.

4.3.43. 5-Methoxy-3-(2-oxo-2-(4-(pyrrolidin-1-yl)piperidin-1-yl)ethyl)benzo[d]oxazol-2(3H)-one (D07)

Off-white solid. Yield: 25%. ^1H NMR (400 MHz, chloroform- d) δ 7.08 (d, $J = 8.6$ Hz, 1H), 6.61 (dd, $J = 8.7$, 2.5 Hz, 1H), 6.58 (d, $J = 2.5$ Hz, 1H), 4.58 (d, $J = 5.6$ Hz, 2H), 4.40 (d, $J = 13.5$ Hz, 1H), 3.92 (d, $J = 13.7$ Hz, 1H), 3.79 (s, 3H), 3.39–3.29 (m, 1H), 3.20 (dd, $J = 14.1$, 11.6, 2.9 Hz, 1H), 2.89–2.78 (m, 1H), 2.63 (d, $J = 6.3$ Hz, 4H), 2.36 (s, 1H), 1.98 (dd, $J = 32.1$, 13.1 Hz, 2H), 1.86–1.78 (m, 4H), 1.00 (t, $J = 7.3$ Hz, 1H). ^{13}C NMR (101 MHz, chloroform- d) δ 163.4, 156.9, 155.0, 136.7, 131.9, 110.3, 107.5, 96.3, 61.12, 56.0, 51.4, 43.7, 40.9, 31.5, 23.2. HRMS (ESI-TOF $^+$) calcd for $\text{C}_{19}\text{H}_{25}\text{N}_3\text{O}_4$ $[\text{M}+\text{H}]^+$ m/z 360.1923, found 360.1918. HPLC: $t_R = 30.14$ min, eluent A-60%, eluent B-40%.

4.3.44. 5-Nitro-3-(2-oxo-2-(4-(pyrrolidin-1-yl)piperidin-1-yl)ethyl)benzo[d]oxazol-2(3H)-one (D08)

Brown solid. Yield: 30%. ^1H NMR (400 MHz, chloroform- d) δ 8.17 (d, $J = 7.9$ Hz, 1H), 8.10 (s, 1H), 7.08 (d, $J = 8.5$ Hz, 1H), 4.76–4.64 (m, 2H), 4.36 (d, $J = 13.6$ Hz, 1H), 3.88 (d, $J = 13.3$ Hz, 1H), 3.35–3.19 (m, 2H), 2.88 (t, $J = 12.2$ Hz, 1H), 2.65 (s, 4H), 2.43–2.27 (m, 2H), 2.00 (dd, $J = 36.9$, 10.3 Hz, 3H), 1.65 (d, $J = 9.1$ Hz, 3H). ^{13}C NMR (101 MHz, chloroform- d) δ 162.5, 154.1, 143.3, 141.9, 136.9, 121.0, 108.8, 106.3, 60.9, 51.4, 43.6, 41.0, 31.5, 30.5, 23.3. HRMS (ESI-TOF $^+$) calcd for $\text{C}_{18}\text{H}_{22}\text{N}_4\text{O}_5$ $[\text{M}+\text{H}]^+$ m/z 375.1668, found 375.1661. HPLC: $t_R = 23.85$ min, eluent A-60%, eluent B-40%.

4.4. Molecular modeling and computations

- Molecular docking. The docking studies were carried out by using the Glide module [43] of Schrödinger Suite (Schrödinger, NY, USA). The chromodomain of CDYL (PDB ID: 2DNT) was prepared using the Protein Preparation Wizard, which assigned bond orders, added hydrogen atoms and removed water molecules. Then the protein was energy minimized using restrained minimization using OPLS3 force field. The grid was generated by defining the hydrophobic cage of CDYL as the box center using Receptor Grid Generation module. For ligands preparation, conformations were generated and energy minimized by using LigPrep module. Extra precision (XP) was used in the Ligand Docking module. Images depicting the proposed binding modes were generated using Maestro 10.6. For virtual screening, the SPECS chemical library was subjected to three levels of docking (HTVS, SP, and XP) using the Virtual Screening Workflow module in Glide. MMGBSA was then calculated after XP docking.
- Molecular dynamic simulations. Desmond module in maestro 10.6 was used. Na^+ and Cl^- ions were added at physiological concentration of 0.15 M to ensure the overall neutrality of the systems. Simulations were then conducted in the OPLS3 force field and a TIP4P explicit solvent model. The final size of the solvated system was close to ~50,000 atoms. A 100 ps recording interval and the NPT ensemble was employed in 300 K and 1.01 bar. The integration time step was set at 2 fs. The model systems were relaxed using a six step default protocol attached to Desmond, and utilized to prepare systems for production-quality simulation. Default settings were used for all other parameters, and the total simulation time was 20 ns. After simulations, the Simulation Interactions Diagram Analysis module was used to monitor energy, RMSD fluctuations, hydrogen bond distances, angles, and van der Waals interactions over the simulation trajectories.

c) Shape screening. For the 2D similarity search, **AK-778/41051004** was used as a template. Pipeline Pilot v7.5 (PP 7.5, Accelrys, Inc.) was used and the fingerprint ECFP-6 was generated for each structure, and similarities were calculated using Tanimoto coefficient, and top 5% of the hits were maintained for manual selection.

4.5. Surface plasmon resonance (SPR)

Briefly, the measurement for binding affinity between chromodomains and their ligands was conducted using Biacore T200 (GE Healthcare) at 25 °C with the flow rate of 30 μ L/min. Recombinant chromodomains were immobilized at pH 4.0–4.5 on the CM5 sensorchip by amine coupling using EDC/NHS, and the immobilization signal ranged from 5000 to 10000 RU. All sensorgrams were reference and blank subtracted. Running buffer was used for blank injections, and bulk effects were corrected using solvent correction. For UNC3866, all buffers used was merely PBSP. For small molecules, they were dissolved in PBSP containing 5% DMSO with 1.5-fold/2-fold dilution series starting from 100 μ M, and the running buffer was PBSP containing 5% DMSO. The association was followed for 60 s and the dissociation for 60 s. For data analyses, the Biacore T200 evaluation software 2.0 (GE Healthcare) was used, and sensorgrams were directly fitted to a 1:1 binding model to calculate related k_a , k_d , and K_D values.

5. Chromodomain clone, expression and purification

5.1. Expression constructs

The chromodomains of CDYL (residues 1–60 of NP_004815), CDYL2 (residues 1–70 of NP_689555), CDY1 (residues 1–65 of NP_733841) and CBX7 (residues 1–62 of NP_783640) were expressed with N-terminal GST-tags in pGEX-6P-1 expression vector.

5.2. Protein expression and purification

All expression constructs were transformed into BL21 *Escherichia coli* (TransGen Biotech, Beijing, China). Protein expression was induced by adding isopropyl β -D-1-thiogalactopyranoside (IPTG) to a final concentration of 0.2 mM when OD600 reached 0.6–0.8, and the culture was further grown at 28 °C for 6 h. Cell were harvested and resuspended in lysis buffer (1 \times PBS, 5 mM DTT, 1 \times EDTA free protease inhibitor cocktail (Roche)). Following sonication and centrifugation, the supernatant was loaded onto a GSTrap FF column (GE Healthcare) that had been pre-equilibrated with 10 column volumes of binding buffer (1 \times PBS, 5 mM DTT) using a AKTA FPLC (GE Healthcare). The column was washed with 10 column volumes of binding buffer and protein was eluted in 100% elution buffer (50 mM Tris, pH 7.5, 150 mM NaCl, 10 mM reduced glutathione) over 10 column volumes. Peak fractions containing the desired protein were pooled and concentrated to 2 mL in Amicon Ultra-15 concentrators, 10,000 molecular weight cut-off (Merck Millipore). Peak fractions were analyzed for purity by SDS-PAGE.

5.3. Affinity tag removal

The N-terminal affinity tag was removed from CDYL, CDYL2, CDY1, and CBX7 by PreScission protease according to manufacturer's recommendations (Beyotime Biotech, Beijing, China). Briefly, purified protein was incubated with PreScission protease at a final concentration of 2 units per 100 μ g tagged protein for 16 h at 4 °C. The cleavage reaction was then passed over a GSTrap FF

column to remove the GST tag. The collected protein was concentrated using Amicon Ultra-15 concentrators, molecular weight 3000 cut-off (Merck Millipore). Proteins were analyzed for purity by SDS-PAGE and stored at –80 °C.

5.4. Cell culture

Human SH-SY5Y and HEK-293T cells were purchased from ATCC and cultured in DMEM supplemented with 10% fetal bovine serum (FBS) in a 37 °C incubator with 5% (v/v) CO₂.

5.5. Cell viability experiments

Cell viability was detected with the CCK-8 kit (Applygen Tech, Beijing) according to the manufacturer's instructions. Briefly, 5000 cells in per well were plated in 96-well plates. After incubated for 24 h, the cells were treated with different concentration of tested compound or DMSO (as negative control) for 24 h. Then 10 μ L CCK-8 was added in per well (100 μ L medium) and incubated at 37 °C for 3 h. Absorbance of each well was determined by a microplate reader (Multiskan GO, Thermo) at a 450 nm wavelength. The results of cytotoxicity were calculated according the formula: $= 100\% \times (\text{OD}_{450} \text{ of tested compound} - \text{OD}_{450} \text{ of medium without cells}) / (\text{OD}_{450} \text{ of DMSO} - \text{OD}_{450} \text{ of medium without cells})$. The IC₅₀ values were calculated using Prism Graphpad software of the triplicate experiment.

5.6. RT-PCR and real-time RT-PCR (qPCR)

Total RNA was isolated from samples with Trizol reagents (Invitrogen) and used for the first strand cDNA synthesis with the Reverse Transcription System (TransGen). Any potential DNA contamination was removed by RNase-free DNase treatment (Promega). Relative quantitation was determined using the ABI PRISM 7500 sequence detection system (Applied Biosystems) that measures real-time SYBR green fluorescence and then calculated by means of the comparative Ct method ($2^{-\Delta\Delta C_t}$) with the expression of GAPDH as an internal control. The sequences of the primers used were provided in [Supplemental Table S2](#).

5.7. Antibodies and reagents

Commercial antibodies used were: anti-CDYL (Sigma, HPA035578), anti- β -actin (Biodragon, B1029), anti-CDYL (Abcam, ab5188), anti-H3K27me3 (Abcam, ab192985), anti-MAP2 (Abcam, ab11267) and anti-Gal 4 (Santa Cruz, sc-510). Protein A beads were from GE Healthcare Biosciences, protease inhibitor mixture cocktail was from Roche Applied Science. Alexa Fluor 488 was from Life Technologies.

5.8. Luciferase reporter assay

SH-SY5Y, or HEK-293T cells in 24-well plates were transfected with luciferase reporter, renilla, and indicated expression constructs. The amount of DNA in each transfection was kept constant by addition of empty vector. 36 h after transfection, the firefly and renilla luciferase were assayed according to the manufacturer's protocol (Promega), and the firefly luciferase activity was normalized to that of renilla luciferase. Each experiment was performed in triplicate and repeated at last three times.

5.9. Western blot

Protein samples were resolved by SDS-PAGE and transferred onto a PVDF membrane (GE Healthcare). The membrane was

blocked by 5% nonfat milk in Tris-buffered saline (TBS) with 0.1% Tween-20 (TBST) for 1 h at room temperature and incubated with appropriate primary antibodies for overnight at 4 °C. The membrane was then washed by TBST for three times and incubated with secondary antibodies (Santa Cruz Biotechnologies) in TBST for 1.5 h at room temperature. After washing by TBST for three times, the immunoreactive bands were visualized using Western Blotting Luminal Reagent (Santa Cruz Biotechnology) according to the manufacturer's recommendation. The bands were quantified by densitometry with ImageJ software.

5.10. Cellular thermal shift assay (CETSA)

The thermal shift assay was performed as previously described [44,45]. Briefly, SH-SY5Y cells were collected and freeze-thawed three times using liquid nitrogen. The lysates were diluted with PBS and divided into two aliquots, with one aliquot being treated with **D03** compound (150 μ M) and the other aliquot as control (DMSO). After 10 min at room temperature, the lysates were heated individually at different temperatures (40–67 °C) for 4 min followed by cooling for 3 min at room temperature. The samples were centrifuged at 13,000 g for 10 min at 4 °C to collect the supernatant. The supernatant was then analyzed by SDS-PAGE followed by Western blot. For the dose-dependent thermal shift assay, the lysates were incubated with various concentrations of **D03** compound (between 0 and 500 μ M) at 55 °C for 4 min. The supernatant was isolated by centrifugation and subjected to immunoblotting analysis of CDYL.

5.11. Chromatin immunoprecipitation (ChIP) and qChIP

ChIP experiments were performed according to the procedure described previously [28,29]. Approximate 1×10^7 SH-SY5Y cells were treated with 150 μ M **D03** compound or DMSO for 24 h. Cells were then fixed with 1% formaldehyde for 10 min at room temperature. The fixed cells were lysed in lysis buffer (1% SDS, 5 mM EDTA and 50 mM Tris-HCl (pH 8.1), plus protease inhibitor cocktail). The lysates were then sonicated with 3×10 cycles (30 s on and off) (Bioruptor, Diagenode) to generate chromatin fragments of ~300 bp in length. Cell debris was removed by centrifugation and supernatant were collected. A dilution buffer (1% Triton X-100, 2 mM EDTA, 20 mM Tris-HCl (pH 8.1), 150 mM NaCl, plus protease inhibitor cocktail) was subsequently applied (1:10 ratio) and the resultant chromatin solution (aliquot 20–40 μ l as the input) was then incubated with control or specific antibodies (3–5 μ g) for 12 h at 4 °C with constant rotation. Protein A/G Sepharose beads (50 μ l of 50% (vol/vol)) were added for incubation of another 2 h. Beads were collected by centrifugation at 500g for 5 min at 4 °C. Beads were sequentially washed with the following buffers for 5 min at 4 °C: TSE I (1% Triton X-100, 0.1% SDS, 2 mM EDTA, 150 mM NaCl, 20 mM Tris-HCl (pH 8.1)); TSE II (1% Triton X-100, 0.1% SDS, 2 mM EDTA, 500 mM NaCl, 20 mM Tris-HCl (pH 8.1)); buffer III (1% Nonidet P-40, 0.25 M LiCl, 1% sodium deoxycholate, 1 mM EDTA and 10 mM Tris-HCl (pH 8.1)); Tris-EDTA buffer. The input and the precipitated DNA-protein complex were decrosslinked at 65 °C for 12 h in elution buffer (1% SDS, 5 mM EDTA, 50 mM NaCl, 20 mM Tris-HCl (pH 8.1), 0.1 mg/mL proteinase K), and DNA was purified using PCR purification kit (Qiagen). Quantification of the precipitated DNA fragments were performed with real-time PCR using primers listed in Supplemental Table S3.

5.12. Primary neuron culture

Hippocampal or cortical explants were isolated from neonatal (P0) C57BL/6 mice of either sex. The explants were digested with

0.25% trypsin (Life Technologies) for 30 min at 37 °C, followed by triturating with a pipette in plating medium (DMEM with 10% FBS). Dissociated neurons were plated onto 35 mm dishes coated with poly-D-lysine (Sigma Aldrich) at a density of 5×10^5 cells per dish. After culturing for 4 h, the medium was changed to Neurobasal medium supplemented with 2% B27 and 0.5 mM GlutaMAX-I (Life Technologies). To test the role of **D03** compound in dendritic branching, neurons were treated with 150 μ M **D03** or DMSO at day 5 in vitro. After 24 h incubation, cells were fixed with 4% paraformaldehyde and subjected to analysis of dendritic branching.

5.13. Immunofluorescence

Primary neurons growing on six-well chamber slides were washed with PBS, fixed in 4% paraformaldehyde, permeabilized with 0.2% Triton X-100 in PBS, blocked with 0.8% BSA, and incubated with MAP2 antibody (Abcam, ab11267) followed by staining with 488-conjugated secondary antibody. The cells were subsequently washed four times and a final concentration of 0.1 μ g/mL 4,6-diamidino-2-phenylindole dihydrochloride (DAPI) was included in the final wash to stain nuclei. Images were visualized and recorded with a confocal microscope (Zeiss LSM880).

5.14. Sholl analysis

Morphology of neurons was analyzed by Sholl analysis. Briefly, fluorescent images were obtained using a confocal microscope and imported into ImageJ software for further analysis. Concentric circles at 10 μ m intervals were drawn around the soma. The number of dendrites crossing each circle was calculated and the data were presented as mean \pm s.e.m.

Author information

L.Y. and Y.L. contributed equally to this work. The manuscript was written through contributions of all authors. All authors have given approval to the final version of the manuscript.

Financial interest

The authors declare no competing financial interest.

Acknowledgements

This study was financially supported by National Natural Science Foundation of China (Grants 31871083 and 81371432 to Z.H., Grants 21572010 and 21772005 to L.Z.). We are grateful for the advice that Dr Jing Wang, the technician at Peking University Health Science Center provided on SPR assays. We also thank Dr. Jinwu Zhou, the field application scientist at Reichert Technologies for his advice on binding assays.

Appendix A. Supplementary data

Supplementary data to this article can be found online at <https://doi.org/10.1016/j.ejmech.2019.111656>.

Abbreviations

CDYL	chromodomain Y-like
CBX7	Chromobox protein homolog 7
PRC1	polycomb repressive complex 1
SAR	structure-activity relationship
EDC	1-ethyl-3-(3-(dimethylamino)propyl)-carbodiimide
NHS	N-Hydroxysuccinimide

TLC	thin-layer chromatography
K ₂ CO ₃	potassium carbonate
TBAI	Tetra- <i>n</i> -butylammonium iodide
EtOAc	ethyl acetate
DCM	dichloromethane
DMF	N,N-Dimethylformamide
BDNF	brain derived neurotrophic factor
SPR	surface plasmon resonance
PCR	polymerase chain reaction
ChIP	chromatin immunoprecipitation
CETSA	cellular thermal shift assay

References

- [1] C.H. Arrowsmith, C. Bountra, P.V. Fish, K. Lee, M. Schapira, Epigenetic protein families: a new frontier for drug discovery, *Nat. Rev. Drug Discov.* 11 (2012) 384–400.
- [2] B.D. Strahl, C.D. Allis, The language of covalent histone modifications, *Nature* 403 (2000) 41–45.
- [3] T.K. Kelly, D.D. De Carvalho, P.A. Jones, Epigenetic modifications as therapeutic targets, *Nat. Biotechnol.* 28 (2010) 1069–1078.
- [4] M.J. Meaney, A.C. Ferguson-Smith, Epigenetic regulation of the neural transcriptome: the meaning of the marks, *Nat. Neurosci.* 13 (2010) 1313–1318.
- [5] A. Portela, M. Esteller, Epigenetic modifications and human disease, *Nat. Biotechnol.* 28 (2010) 1057–1068.
- [6] J.L. Anglin, Y. Song, A medicinal chemistry perspective for targeting histone H3 lysine-79 methyltransferase DOT1L, *J. Med. Chem.* 56 (2013) 8972–8983.
- [7] S.R. Daigle, E.J. Olhava, C.A. Therkelsen, A. Basavapathruni, L. Jin, P.A. Boriack-Sjodin, C.J. Allain, C.R. Klaus, A. Raimondi, M.P. Scott, N.J. Waters, R. Chesworth, M.P. Moyer, R.A. Copeland, V.M. Richon, R.M. Pollock, Potent inhibition of DOT1L as treatment of MLL-fusion leukemia, *Blood* 122 (2013) 1017–1025.
- [8] Y. Yao, P. Chen, J. Diao, G. Cheng, L. Deng, J.L. Anglin, B.V. Prasad, Y. Song, Selective inhibitors of histone methyltransferase DOT1L: design, synthesis, and crystallographic studies, *J. Am. Chem. Soc.* 133 (2011) 16746–16749.
- [9] S.K. Knutson, N.M. Warholc, T.J. Wigle, C.R. Klaus, C.J. Allain, A. Raimondi, M. Porter Scott, R. Chesworth, M.P. Moyer, R.A. Copeland, V.M. Richon, R.M. Pollock, K.W. Kuntz, H. Keilhack, Durable tumor regression in genetically altered malignant rhabdoid tumors by inhibition of methyltransferase EZH2, *Proc. Natl. Acad. Sci. U. S. A.* 110 (2013) 7922–7927.
- [10] P.P. Kung, P. Bingham, A. Broun, M. Collins, Y.L. Deng, D. Dinh, C. Fan, K.S. Gajiwala, R. Grantner, H.J. Gukasyan, W. Hu, B. Huang, R. Kania, S.E. Kephart, C. Krivacic, R.A. Kumpf, P. Khamphavong, M. Kraus, W. Liu, K.A. Maegley, L. Nguyen, S. Ren, D. Richter, R.A. Rollins, N. Sach, S. Sharma, J. Sherrill, J. Spangler, A.E. Stewart, S. Sutton, S. Uryu, D. Verhelle, H. Wang, S. Wang, M. Wythes, S. Xin, S. Yamazaki, H. Zhu, J. Zhu, L. Zehnder, M. Edwards, Optimization of orally bioavailable enhancer of zeste homolog 2 (EZH2) inhibitors using ligand and property-based design strategies: identification of development candidate (R)-5,8-Dichloro-7-(methoxy(oxetan-3-yl)methyl)-2-((4-methoxy-6-methyl-2-oxo-1,2-dihydropyridin-3-yl)methyl)-3,4-dihydroisoquinolin-1(2H)-one (PF-06821497), *J. Med. Chem.* 61 (2018) 650–665.
- [11] M.T. McCabe, H.M. Ott, G. Ganji, S. Korenchuk, C. Thompson, G.S. Van Aller, Y. Liu, A.P. Graves, A. Della Pietra 3rd, E. Diaz, L.V. LaFrance, M. Mellinger, C. Duquenne, X. Tian, R.G. Kruger, C.F. McHugh, M. Brandt, W.H. Miller, D. Dhanak, S.K. Verma, P.J. Tummino, C.L. Creasy, EZH2 inhibition as a therapeutic strategy for lymphoma with EZH2-activating mutations, *Nature* 492 (2012) 108–112.
- [12] R.G. Vaswani, V.S. Gehling, L.A. Dakin, A.S. Cook, C.G. Nasveschuk, M. Duplessis, P. Iyer, S. Balasubramanian, F. Zhao, A.C. Good, R. Campbell, C. Lee, N. Cantone, R.T. Cummings, E. Normant, S.F. Bellon, B.K. Albrecht, J.C. Harmange, P. Trojer, J.E. Audia, Y. Zhang, N. Justin, S. Chen, J.R. Wilson, S.J. Gamblin, Identification of (R)-N-((4-Methoxy-6-methyl-2-oxo-1,2-dihydropyridin-3-yl)methyl)-2-methyl-1-(1-(2,2,2-trifluoroethyl)piperidin-4-yl)ethyl)-1H-indole-3-carboxamide (CPI-1205), a potent and selective inhibitor of histone methyltransferase EZH2, suitable for phase I clinical trials for B-cell lymphomas, *J. Med. Chem.* 59 (2016) 9928–9941.
- [13] P.A. Marks, Discovery and development of SAHA as an anticancer agent, *Oncogene* 26 (2007) 1351.
- [14] L. Stimson, O. Khan, S. Fotheringham, V. Wood, N.B. La Thangue, HDAC inhibitor-based therapies and haematological malignancy, *Ann. Oncol.* 20 (2009) 1293–1302.
- [15] M. New, H. Olzscha, N.B. La Thangue, HDAC inhibitor-based therapies: can we interpret the code? *Mol. Oncol.* 6 (2012) 637–656.
- [16] M.G.J. Baud, E. Lin-Shiao, T. Cardote, C. Tallant, A. Pschibul, K.H. Chan, M. Zengerle, J.R. Garcia, T.T. Kwan, F.M. Ferguson, A. Ciulli, Chemical biology: A bump-and-hole approach to engineer controlled selectivity of BET bromodomain chemical probes, *Science* 346 (2014) 638–641.
- [17] X. Dai, W. Gan, X. Li, S. Wang, W. Zhang, L. Huang, S. Liu, Q. Zhong, J. Guo, J. Zhang, T. Chen, K. Shimizu, F. Beca, M. Blattner, D. Vasudevan, D.L. Buckley, J. Qi, L. Buser, P. Liu, H. Inuzuka, A.H. Beck, L. Wang, P.J. Wild, L.A. Garraway, M.A. Rubin, C.E. Barbieri, K.K. Wong, S.K. Muthuswamy, J. Huang, Y. Chen, J.E. Bradner, W. Wei, Prostate cancer-associated SPOP mutations confer resistance to BET inhibitors through stabilization of BRD4, *Nat. Med.* 23 (2017) 1063–1071.
- [18] B.T. Lahn, D.C. Page, Retroposition of autosomal mRNA yielded testis-specific gene family on human Y chromosome, *Nat. Genet.* 21 (1999) 429.
- [19] C. Caron, C. Pivot-Pajot, L.A. van Grunsven, E. Col, C. Lestrat, S. Rousseaux, S. Khochbin, Cdy1: a new transcriptional co-repressor, *EMBO Rep.* 4 (2003) 877–882.
- [20] W. Fischle, H. Franz, S.A. Jacobs, C.D. Allis, S. Khorasanizadeh, Specificity of the chromodomain Y chromosome family of chromodomains for lysine-methylated ARK(S/T) motifs, *J. Biol. Chem.* 283 (2008) 19626–19635.
- [21] H. Franz, K. Mosch, S. Soeroes, H. Urlaub, W. Fischle, Multimerization and H3K9me3 binding are required for CDYL1b heterochromatin association, *J. Biol. Chem.* 284 (2009) 35049–35059.
- [22] Y. Zhang, X. Yang, B. Gui, G. Xie, D. Zhang, Y. Shang, J. Liang, Corepressor protein CDYL functions as a molecular bridge between polycomb repressor complex 2 and repressive chromatin mark trimethylated histone lysine 27, *J. Biol. Chem.* 286 (2011) 42414–42425.
- [23] Y. Liu, S. Liu, S. Yuan, H. Yu, Y. Zhang, X. Yang, G. Xie, Z. Chen, W. Li, B. Xu, L. Sun, Y. Shang, J. Liang, Chromodomain protein CDYL is required for transmission/restoration of repressive histone marks, *J. Mol. Cell Biol.* 9 (2017) 178–194.
- [24] B.T. Lahn, Z.L. Tang, J. Zhou, R.J. Barndt, M. Parvinen, C.D. Allis, D.C. Page, Previously uncharacterized histone acetyltransferases implicated in mammalian spermatogenesis, *Proc. Natl. Acad. Sci. U. S. A.* 99 (2002) 8707–8712.
- [25] S. Liu, H. Yu, Y. Liu, X. Liu, Y. Zhang, C. Bu, S. Yuan, Z. Chen, G. Xie, W. Li, B. Xu, J. Yang, L. He, T. Jin, Y. Xiong, L. Sun, X. Liu, C. Han, Z. Cheng, J. Liang, Y. Shang, Chromodomain protein CDYL acts as a crotonyl-CoA hydratase to regulate histone crotonylation and spermatogenesis, *Mol. Cell* 67 (2017) 853–866 e855.
- [26] C. Qi, S. Liu, R. Qin, Y. Zhang, G. Wang, Y. Shang, Y. Wang, J. Liang, Coordinated regulation of dendrite arborization by epigenetic factors CDYL and EZH2, *J. Neurosci.* 34 (2014) 4494–4508.
- [27] R. Qin, S. Cao, T. Lyu, C. Qi, W. Zhang, Y. Wang, CDYL deficiency disrupts neuronal migration and increases susceptibility to epilepsy, *Cell Rep.* 18 (2017) 380–390.
- [28] Y. Liu, S. Lai, W. Ma, W. Ke, C. Zhang, S. Liu, Y. Zhang, F. Pei, S. Li, M. Yi, Y. Shu, Y. Shang, J. Liang, Z. Huang, CDYL suppresses epileptogenesis in mice through repression of axonal Nav1.6 sodium channel expression, *Nat. Commun.* 8 (2017) 355.
- [29] Y. Liu, M. Li, M. Fan, Y. Song, H. Yu, X. Zhi, K. Xiao, S. Lai, J. Zhang, X. Jin, Y. Shang, J. Liang, Z. Huang, Chromodomain Y-like protein-mediated histone crotonylation regulates stress-induced depressive behaviors, *Biol. Psychiatry* 85 (2019) 635–649.
- [30] S.V. Frye, The art of the chemical probe, *Nat. Chem. Biol.* 6 (2010) 159.
- [31] R.J. Eisert, S.A. Kennedy, M.L. Waters, Investigation of the beta-sheet interactions between dHP1 chromodomain and histone 3, *Biochemistry* 54 (2015) 2314–2322.
- [32] S.A. Baril, A.L. Koenig, M.W. Krone, K.I. Albanese, C.Q. He, G.Y. Lee, K.N. Houk, M.L. Waters, E.M. Brustad, Investigation of trimethyllysine binding by the HP1 chromodomain via unnatural amino acid mutagenesis, *J. Am. Chem. Soc.* 139 (2017) 17253–17256.
- [33] C. Simhadri, K.D. Daze, S.F. Douglas, T.T. Quon, A. Dev, M.C. Gignac, F. Peng, M. Heller, M.J. Boulanger, J.E. Wulff, F. Hof, Chromodomain antagonists that target the polycomb-group methyllysine reader protein chromobox homolog 7 (CBX7), *J. Med. Chem.* 57 (2014) 2874–2883.
- [34] J.I. Stuckey, C. Simpson, J.L. Norris-Drouin, S.H. Cholensky, J. Lee, R. Pasca, N. Cheng, B.M. Dickson, K.H. Pearce, S.V. Frye, L.I. James, Structure-activity relationships and kinetic studies of peptidic antagonists of CBX chromodomains, *J. Med. Chem.* 59 (2016) 8913–8923.
- [35] C. Ren, S.G. Smith, K. Yap, S. Li, J. Li, M. Mezei, Y. Rodriguez, A. Vincek, F. Aguilo, M.J. Walsh, M.M. Zhou, Structure-guided discovery of selective antagonists for the chromodomain of polycomb repressive protein CBX7, *ACS Med. Chem. Lett.* 7 (2016) 601–605.
- [36] J. Vandamme, P. Volkel, C. Rosnoblet, P. Le Faou, P.O. Angrand, Interaction proteomics analysis of polycomb proteins defines distinct PRC1 complexes in mammalian cells, *Mol. Cell. Proteom.* 10 (2011). M110 002642.
- [37] L. Morey, L. Aloia, L. Cozzuto, A.S. Benitah, L. Di Croce, RYBP and Cbx7 define specific biological functions of polycomb complexes in mouse embryonic stem cells, *Cell Rep.* 3 (2013) 60–69.
- [38] J.I. Stuckey, B.M. Dickson, N. Cheng, Y. Liu, J.L. Norris, S.H. Cholensky, W. Tempel, S. Qin, K.G. Huber, C. Sagum, K. Black, F. Li, X.P. Huang, B.L. Roth, B.M. Baughman, G. Senisterra, S.G. Pattenden, M. Vedadi, P.J. Brown, M.T. Bedford, J. Min, C.H. Arrowsmith, L.I. James, S.V. Frye, A cellular chemical probe targeting the chromodomains of Polycomb repressive complex 1, *Nat. Chem. Biol.* 12 (2016) 180–187.
- [39] K.D. Barnash, K.N. Lamb, J.I. Stuckey, J.L. Norris, S.H. Cholensky, D.B. Kireev, S.V. Frye, L.I. James, Chromodomain ligand optimization via target-class directed combinatorial repurposing, *ACS Chem. Biol.* 11 (2016) 2475–2483.

- [40] J. Behnke, A. Cheedalla, V. Bhatt, M. Bhat, S. Teng, A. Palmieri, C.C. Windon, S. Thakker-Varia, J. Alder, Neuropeptide VGF promotes maturation of hippocampal dendrites that is reduced by single nucleotide polymorphisms, *Int. J. Mol. Sci.* 18 (2017).
- [41] J. Alder, S. Thakker-Varia, D.A. Bangasser, M. Kuroiwa, M.R. Plummer, T.J. Shors, I.B. Black, Brain-derived neurotrophic factor-induced gene expression reveals novel actions of VGF in hippocampal synaptic plasticity, *J. Neurosci.* 23 (2003) 10800–10808.
- [42] A. Bahi, J.L. Dreyer, Viral-mediated overexpression of the Myelin Transcription Factor 1 (MyT1) in the dentate gyrus attenuates anxiety- and ethanol-related behaviors in rats, *Psychopharmacology* 234 (2017) 1829–1840.
- [43] T.A. Halgren, R.B. Murphy, R.A. Friesner, H.S. Beard, L.L. Frye, W.T. Pollard, J.L. Banks, Glide: a new approach for rapid, accurate docking and scoring. 2. Enrichment factors in database screening, *J. Med. Chem.* 47 (2004) 1750–1759.
- [44] D. Martinez Molina, R. Jafari, M. Ignatushchenko, T. Seki, E.A. Larsson, C. Dan, L. Sreekumar, Y. Cao, P. Nordlund, Monitoring drug target engagement in cells and tissues using the cellular thermal shift assay, *Science* 341 (2013) 84–87.
- [45] R. Jafari, H. Almqvist, H. Axelsson, M. Ignatushchenko, T. Lundback, P. Nordlund, D. Martinez Molina, The cellular thermal shift assay for evaluating drug target interactions in cells, *Nat. Protoc.* 9 (2014) 2100–2122.